ANCHORAGE STRENGTH OF FIBER REINFORCED POLYMERS

A THESIS SUBMITTED TO
THE GRADUATE SCHOOL OF NATURAL AND APPLIED SCIENCES
OF
MIDDLE EAST TECHNICAL UNIVERSITY

BY

ÜMİT SERDAR ÇAMLI

IN PARTIAL FULFILLMENT OF THE REQUIREMENTS
FOR
THE DEGREE OF MASTER OF SCIENCE
IN
CIVIL ENGINEERING

NOVEMBER 2005

Approval of the Graduate School of Natural and Applied Sciences

Prof. Dr. Canan ÖZGEN
Director

I certify that this thesis satisfies all the requirements as a thesis for the degree of Master of Science

Prof. Dr. Erdal ÇOKCA
Head of Department

This is to certify that we have read this thesis and that in our opinion it is fully adequate, in scope and quality, as a thesis for the degree of Master of Science

Asst. Prof. Dr. Barış BİNİCİ
Supervisor

Examining Committee Members

Prof. Dr. Güney ÖZCEBE	(METU)	
Asst. Prof. Dr. Barış BİNİCİ	(METU)	
Assoc. Prof. Dr. Uğurhan AKYÜZ	(METU)	
Asst. Prof. Dr. Erdem CANBAY	(METU)	
Dr. Bekir Afşin CANBOLAT	(YÜKSEL PROJE)	

I hereby declare that all information in this document has been obtained and presented in accordance with academic rules and ethical conduct. I also declare that, as required by these rules and conduct, I have fully cited and referenced all material and results that are not original to this work.

Name, Last Name: Ümit Serdar ÇAMLI

Signature :

ABSTRACT

ANCHORAGE STRENGTH OF FIBER REINFORCED POLYMERS

Çamlı, Ümit Serdar
M.Sc., Department of Civil Engineering
Supervisor: Asst. Prof. Dr. Barış Binici

November 2005, 83 pages

Fiber reinforced polymers (FRPs) have gained popularity in upgrade projects for reinforced concrete structural elements within the last decade because of its ease of application and high strength-to-weight ratio. In the design of an effective retrofitting solution by means of an FRP system, the anchorage capacity has an important role. This study presents the results of an experimental program conducted to determine the strength of carbon fiber reinforced polymers (CFRPs) bonded to concrete prisms or hollow clay tiles that are finished with or without plaster. In the experimental program, different types of anchorage methods were tested in a double shear push-out test setup. A simple and effective strength model is proposed for strip type anchorages based on the existing analytical models and experimental observations from this study. This new model is suitable for determining the design capacity of CFRP-to-concrete and CFRP-to-hollow clay tile joints with or without plaster and accounts for the presence of embedment and concrete strength. Obtained results by using this model were found to closely match with the experimental observations.

Keywords: Fiber Reinforced Polymers (FRPs), Plaster, Hollow Clay Tile, Anchorage Strength Model, Anchorage Types

ÖZ

LİFLİ POLİMERLERİN ANKARAJ DAYANIMLARI

Çamlı, Ümit Serdar
Yüksek Lisans, İnşaat Mühendisliği Bölümü
Tez Yöneticisi: Y. Doç. Dr. Barış Binici

Kasım 2005, 83 sayfa

Lifli polimerler, kolay uygulanabilmesi ve yüksek dayanım-ağırlık oranı sayesinde son yıllarda güçlendirme projelerinde sıklıkla kullanılmaya başlanmıştır. Lifli polimerler kullanılarak yapılan güçlendirme projelerinin hesaplamalarında ankraj dayanımının önemli bir rolü vardır. Bu çalışmada, beton veya tuğla elemanların sıvalı veya sıvasız yüzeylerine yapıştırılmış karbon lifli polimerlerin kesme dayanımları üzerine deneysel bir program sunulmuştur. Bu deneysel çalışmada çift eksen çekme deney düzeneği kullanılarak değişik ankraj metodları denenmiştir. Mevcut çalışmalara ve tarafımızca yapılan deneysel gözlemlere dayanılarak şerit tipi ankraj çeşitleri için kullanışlı bir ankraj dayanım modeli oluşturulmuştur. Bu, yüzeyleri sıvalı veya sıvasız olan beton veya tuğla elemanlar ile lifli polimer birleşim kapasiteleri için gömme ve beton dayanımlarını da hesaba katan uygun bir modeldir. Modelden elde edilen sonuçlar deneysel gözlemler ile uyuşmaktadır.

Anahtar Kelimeler: Lifli Polimer (LP), Sıva, Tuğla, Ankaraj Dayanımı Modeli, Ankaraj Çeşitleri

ACKNOWLEDGEMENTS

I would like to express my sincere thanks and appreciation to Asst. Prof. Dr. Barış Binici, who is the supervisor of this study. His suggestions, guidance, and support encouraged me to complete this study. It was a great honor and pleasure to work with him.

I also would like to convey my endless appreciation to my parents, İpek and Kemal Çamlı, my brother Uğur Çamlı, and my sister Dilek Çamlı for their confidence in me and infinite support during the project. Knowing the fact that they were always behind of me increased my success significantly.

I also would like to thank other members of the faculty who have contributed to this study in various ways; in lectures and suggestions.

METU Structural Mechanics Laboratory staff deserves my sincere thanks due to their great help and effort for this study.

This study was conducted under the financial support from the Scientific and Technical Research Council of Turkey (TÜBİTAK, İÇTAG I-597).

TABLE OF CONTENTS

LIST OF TABLES

TABLE

LIST OF FIGURES

FIGURE

LIST OF SYMBOLS

f_{frp}: FRP sheet tensile strength

t_{frp}: FRP sheet thickness

b_{frp}: FRP sheet width

L_{frp}: FRP sheet bond length

A_{frp}: FRP sheet area

E_{frp}: Young`s modulus of FRP sheet

σ_{frp}: Stress of FRP sheet

f_c: Concrete or HCT specimen compressive strength

f_{ct}: Concrete specimen tensile strength

b_c: Concrete or HCT specimen width

E_c: Young`s modulus of concrete or HCT blocks

σ_c: Stress of concrete or HCT blocks

t_p: Plaster thickness

f_p: Plaster compressive strength

τ_{fa}: Ultimate shear strength of adhesive-FRP interface

τ_{fp}: Ultimate shear strength of plaster-concrete interface

δ_p: Slip displacement of plaster at corresponding ultimate shear strength of plaster-concrete interface

δ_a: Slip displacement of adhesive at corresponding ultimate shear strength of adhesive-FRP interface

δ_{up}: Ultimate slip displacement of plaster

δ_{ua}: Ultimate slip displacement of adhesive

u_c: Displacement of concrete or HCT block

u_{frp}: Displacement of CFRP

δ: Slip displacement of the anchorage

δ_1: Slip displacement of the plaster

δ_2: Slip displacement of the adhesive

τ: Shear strength of the anchorage

σ : Stress of the anchorage

L_e: Effective anchor bond length

a: Debonding length of anchor

E_1: Fracture energy of exact solution

E_2: Fracture energy of approximate solution

P_{test}: Ultimate load capacity of anchorage

P_{frp}: Ultimate load capacity of FRP sheet

CHAPTER 1

INTRODUCTION

1.1 INTRODUCTION

Structures are designed and constructed to supply sufficient capacity against vertical and lateral load demands with the purposes of providing life safety and preventing collapse. However, many examples of catastrophic results such as failure or damage of buildings, bridge piers etc. are seen all over the world. These can be due to intentionally or unintentionally created deficiencies during service life and lack of control that needs to be provided both at design and construction stages.

The main reasons of deficiencies in the structure are: (i) changes in displacement demands on the structure and individual component, (ii) changes in capacity requirements of the structural elements, (iii) insufficient building code provisions and (iv) design/construction errors. In Turkey, vast amount of structures in earthquake prone zones are far from being earthquake resistant and they have most of the deficiencies listed above, hence they need to be retrofitted.

There is a vast amount of experimental and analytical work on retrofitting structural components presented in the literature. Addition of shear walls is one of the most commonly used retrofit methods in Turkey. Although structures retrofitted with RC walls proved to perform satisfactorily in earthquakes, they have important disadvantages such as being difficult to apply and requiring evacuation of the occupants.

As part of a comprehensive research project, Özcebe et al. [1] conducted a set of experiments on FRP strengthened hollow clay tile (HCT) infill walls to

develop a new strengthening technique. This novel technique employed diagonally installed FRP strips directly onto the plastered wall surfaces to enhance the lateral strength and deformation capacity of reinforced concrete frames with infill walls. In addition, drill through FRP dowels are used at various locations along the FRP strips to reduce the possible debonding (Figure 1.1). The experimental results showed that FRP retrofit of infill walls can result in an enhanced seismic performance of deficient RC frames with hollow clay tile (HCT) infills. One important observation from these experiments was the progressive debonding of FRPs between anchor dowels, once a crack formed along mortar joints. Therefore, it is important to know the required bond length to develop the diagonally installed FRPs prior to reaching the ultimate state of the system.

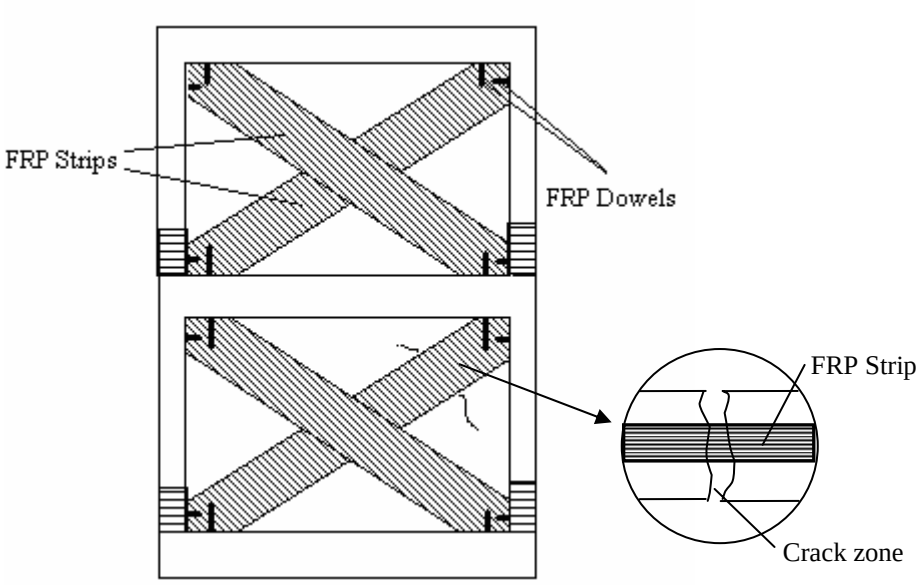

Figure 1.1 Test Specimen of the Study of Özcebe et al. [1]

External bonding of steel plates in retrofitting deficient beams has been used for nearly four decades [2]. High labor cost, low strength-to-weight ratio, and difficulties in application of external bonded steel plates are the main disadvantages. Fiber reinforced polymers (FRPs), which were originally used

in defense and aerospace industries, have become popular in civil engineering applications since 1990s due to increased production with reduced cost. Although application procedure of these polymers are similar to the strengthening with steel plates, fiber reinforced polymers have replaced the use of steel plates due to their ease of application and high strength-to-weight ratio.

Externally bonded FRP sheets are used in strengthening of the components of a structure to increase flexural, shear, and axial capacities. Beams in a structure can be strengthened for shear and flexural loads using FRP sheets. In Figure 1.2, failure modes of beams strengthened in flexure are presented [3]. It can be observed that apart from FRP rupture and concrete crushing failure modes, all of the failure modes are associated with FRP debonding initiating from a crack. Therefore, it can be stated that bond strength of FRPs needs to be estimated safely prior to the design of an effective FRP retrofit. Some of the important FRP retrofit applications outlined above show that a thorough understanding of strength of FRPs bonded to concrete is a prerequisite for successful applications of FRPs. Especially in countries with little or no experience with FRPs, detailed experimental studies need to be conducted that suit the needs of the construction practice.

1.2 LITERATURE REVIEW

With increasing popularity of the fiber reinforced polymers in structural engineering projects, vast amount of studies have been conducted all over the world. In this section, some of the important studies in the literature, as they relate to this study, are presented.

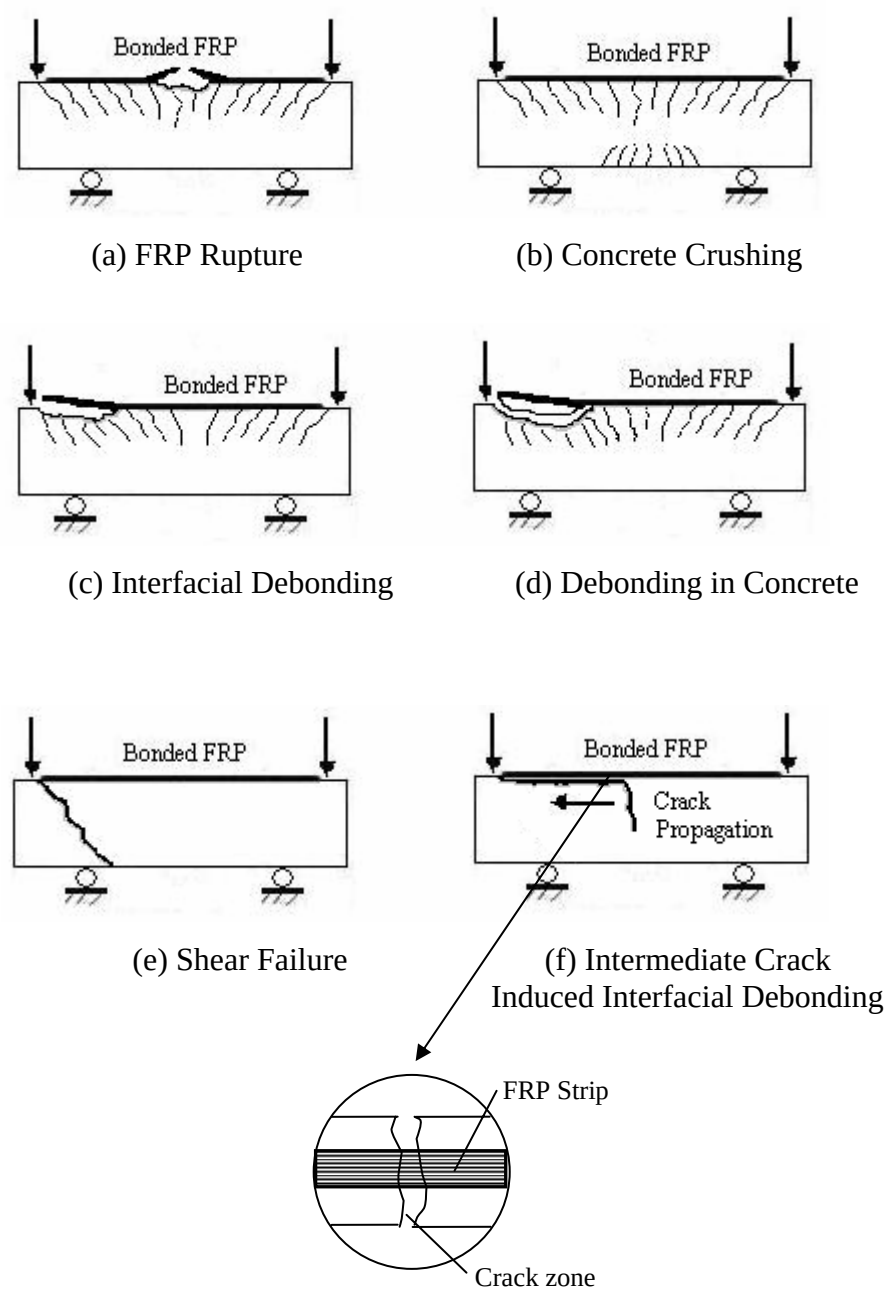

Figure 1.2 Classification of Failure Modes of Beams

Studies in the literature can be grouped mainly into two categories: experimental and analytical studies, although some of the researchers conducted both, subsequently. A brief summary of the existing experimental studies on FRP bond capacity and behavior, conducted using various test setups, are presented next.

1.2.1 Experimental Studies

Chajes et al. [4] studied the bond strength of FRP-concrete interface and force transfer from composite material plate to concrete, employing single shear test-setup. The parameters of the experiments were the effect of the surface preparation of concrete, adhesive type, and concrete strength in case of the constant bond length. In addition, effect of the bond length was also investigated. According to the test results, mechanical abrasion of the concrete surface was recommended which resulted in the highest average stress at failure during the tests.

Täljsten [5] conducted a set of single shear tests and studied the anchorage length of steel and CFRP plates bonded to concrete. It was pointed out that effective anchorage length may differ substantially for steel and CFRP applications. According to the strain measurements, it was also observed that strain limit the concrete was the governing factor for failure. A derivation of the shear stresses based on elastic closed form solutions was presented in the adhesive layer expressed for both steel and CFRP plates bonded to concrete.

Yao et al. [6] carried out an experimental study on FRP bonded to concrete using near end supported single shear tests. These tests were conducted with the aim of verifying the accuracy of the bond strength model of Chen and Teng [22] and examining the reliability of the near end supported single shear pull tests. Bond length, concrete strength, FRP-to-concrete width ratio, and support height were the investigated parameters. Test results showed that model of Chen and Teng [22] was conservative for extreme values of FRP-to-concrete width ratio.

Dai et al. [7] studied the bond transfer mechanisms to improve the load carrying capacity of the bonded joints using single shear test setup. As a conclusion, the researchers pointed out that decreasing the shear stiffness of adhesive improved the ultimate shear strength. In addition, it was argued that

increase of FRP bond length increased the interfacial strength and deformation capacities.

Binici [8] conducted a set of double shear tests to determine the behavior of CFRP laminated bonded to concrete prisms and cylinders. CFRP bond length was the parameter of the experimental study. The ultimate loads, maximum slip displacements, and strain profiles along the bond length were reported. An analytical model was proposed to determine the ultimate shear strength of CFRP at the end of the tests and comparison of the test results with the predicted shear strength was performed. Binici [8] indicated that for efficient utilization of fiber reinforced polymers in structural upgrade applications, anchoring systems were required.

De Loranzis et al. [9] conducted beam tests to examine the flexural bond capacity of FRPs and to determine the effects of bond length, size effect, FRP stiffness, and sheet width on the FRP bond capacity. As a result, design expressions for peeling stresses, effective bond length, and FRP ultimate strain, which can be used in controlling bond failure, was proposed. Researchers pointed out that failure occurred at concrete adhesive interface without any significant damage of concrete and added that the concrete strength did not affect the ultimate load.

Özdemir [10] conducted an experimental program on FRP dowels pull-out capacities using a conventional pullout test setup. These dowels can be used in anchorage applications of the FRP bonded to the hollow clay tile walls. During the tests, effects of concrete strength, anchorage depth, anchorage diameter, and FRP width were investigated. Researcher proposed an equation to predict the tensile capacity of CFRP anchor dowels and defined an effective depth of about 100 mm for the CFRP anchor dowels embedded to concrete.

Kobayashi et al. [11] conducted studies on strengthening with FRP laminates and attempted to develop a simple wrapping system for columns surrounded

with wing, shear, and tile walls. Fan type CFRP anchors, similar to examined in this study, was used to make a connection between wrapped CFRP laminates and structure. It was reported that with a carefully designed detail at anchorage zone a great amount of tensile capacity could be transferred between wrapped CFRP laminates and structure.

1.2.2 Analytical Studies

Analytical studies on FRP bond are based on two models such as bond-strength and bond-slip. Bond-slip models are more suitable for detailed finite element analysis, hence they are not design oriented. To name a few of these models, Dai et al. [12] developed a simple method to determine a nonlinear bond-slip model of the FRP-to-concrete interfaces. Using this model, interface behavior and ultimate shear strength were obtained for different types of FRP laminates and adhesives. Experimental results showed that interfacial fracture energy was affected by FRP stiffness, mechanical properties of adhesive, and concrete strength. On the other hand, decreases of the FRP stiffness led to the improvement of the interfacial load transfer capacity.

Nabaka et al. [13] conducted a double shear experimental study to obtain local bond-slip behavior between different types of concrete and FRP interfaces, which were the primary variables in the program. A new model was presented for bond stress-slip relationship. Numerical simulations were compared with experimental results, yielding good match between the two. The results showed that fiber stiffness can greatly affect both ultimate shear strength and stress distribution at the interfaces.

Lu et al. [14] presented a review of existing bond strength and bond slip models and examined these models with the results of 253 FRP-to–concrete pull tests to show that a more accurate model for FRP-to-concrete bonded joints was required. They developed a model based on the bond-slip model by using meso-scale finite element model and reported that the initial stiffness of

the bond slip curve, larger than the second stiffness at the peak stress, decreases quickly with the increase of the bond stress. Assuming initial stiffness as infinite, according to the fact that initial stress of stress slip curve is much larger than second stiffness, researchers proposed a simple bond-slip model. In the study, a bilinear model was also derived by using a bilinear bond-slip model. Through comparisons with test database composed of 253 tests, all three models predict both the bond strength and strain distributions in the FRP plate accurately.

Theoretical models developed to determine bond strength of FRP bonded to structural materials (concrete or masonry) based on the pull or pushout tests are called bond-strength models. Some of the important bond-strength models are given in this section.

Malek et al. [15] examined local failures between FRP plates and concrete beams, developed a closed form solution for calculating shear and peeling stresses at the interface of FRP and concrete by using linear elastic material model. Predicted results of the analytical model was compared both with finite element model and test results.

Brosens and Gemert [16] derived a bond strength model including a width effect coefficient which was based on the FRP width to concrete specimen width ratio. Researchers also conducted pull tests including the parameters: CFRP width, number of CFRP plies, and CFRP bond length. Their analytical model lacked the concept of effective bond length, resulting in unsafe strength estimations for large bond lengths.

Wu et al. [17] derived expressions for the maximum transferable load, interfacial stress distribution, and initiation and propagation of interfacial cracking by using two different nonlinear stress-slip relationships. They also performed numerical simulations of the model and made comparisons with finite element analysis. Researchers showed the fact that the stress transfer and

debonding behaviors can be different for pull-pull and pull-push joints, which were two loading types in both single and double shear test.

Yuan et al. [18] developed an analytical model using closed form expressions for estimating FRP-to-concrete bonded joint capacity and behavior. In this study, expressions for the interfacial shear-stress distribution and load-displacement response were derived for different loading stages, bond length, and plate stiffness effects and were presented with help of the analytical model. Researchers indicated that the ultimate load of bonded joints increased with the bond length and axial stiffness of the FRP laminates stiffness. Their model helps to evaluate the full range load-displacement behavior of a pull-push joint with a nonlinear interface material response, but the approach is not design oriented.

Maeda et al. [19] conducted an experimental program on the FRP-to-concrete bonded joints using double shear tests. Bond length and FRP thickness were the parameters in the experimental program. As a result of the study, researchers obtained that increase of bond length beyond a value of about 100 mm did not affect the ultimate stress of the FRP-to-concrete interface. Furthermore, researchers derived an empirical model that presented the ultimate shear strength as:

$$\tau = 110.2\ 10^{-6} t_p E_p \tag{1.1}$$

where t_p and E_p were thickness (mm) and Young`s modulus (GPa) of the bonded plate, respectively. Ultimate bond strength P_u was obtained by multiplying ultimate shear strength with b_p and L_e. Effective length (L_e) is given in Eq.(1.2):

$$L_e = e^{6.13-0.58\ \ln(t_p E_p)} \tag{1.2}$$

In Chapter 3, the performance of their model in evaluating the strength of specimens in this study will be examined.

Ueda et al. [20] conducted experiments on FRPs bonded to concrete using a double shear setup and developed an extremely simple empirical relationship for ultimate bond strength given in Eq.(1.3).

$$\tau = 0.19 t_{frp} E_{frp} \tag{1.3}$$

In Eq (1.3), t_{frp} is the FRP laminate width and E_{frp} is the FRP laminate stiffness. Furthermore, similar to the findings of Maeda et. al. [19], an effective bond length of 100 mm was observed in these experiments.

Neubauer and Rostásy [21] examined CFRP sheets bonded to concrete specimens to derive the fracture energy of the bond, G_f, given as:

$$G_f = k_p c_f f_{ct} \tag{1.4}$$

in which f_{ct} is concrete tensile strength, c_f and k_p are secondary effect and width ratio factors obtained from 70 tests. They also modified Holzenkämpfer`s model [24] to determine design orientation model. The model takes the form in Eq.(1.5)

$$P_u = \begin{cases} 0.64 k_p b_{frp} \sqrt{E_{frp} t_{frp} f_{ct}} & \text{if} \quad L \geq L_e \\ 0.64 k_p b_{frp} \sqrt{E_{frp} t_{frp} f_{ct}} \, \dfrac{L}{L_e}\left(2 - \dfrac{L}{L_e}\right) & \text{if} \quad L < L_e \end{cases} \tag{1.5a}$$

$$L_e = \sqrt{\frac{E_{frp} t_{frp}}{2 f_{ct}}} \tag{1.5b}$$

The performance of their model in evaluating the strength of specimens tested in this study will be presented in Chapter 3.

Chen and Teng [22] presented a state-of-the-art review of anchorage strength experiments and models to estimate anchorage strength of both FRP and steel plates bonded to concrete. Finally, these researchers proposed a new model that was suitable for both FRP-to-concrete and steel-to-concrete bonded joints based on the existing fracture mechanic analysis and experimental

observations that were presented in their study. They indicated that both the anchorage strength and the effective length can be correctly predicted by using their model given in Eq.(1.6).

$$P_u = 0.427\beta_l \beta_w \sqrt{f_c} b_{frp} L_{eff} \tag{1.6a}$$

$$L_{eff} = \sqrt{\frac{E_{frp} t_{frp}}{\sqrt{f_c}}} \tag{1.6b}$$

$$\beta_l = \begin{cases} 1 & \text{if} \quad L \geq L_{eff} \\ \sin(\frac{\pi L}{2L_{eff}}) & \text{if} \quad L < L_{eff} \end{cases} \tag{1.6c}$$

$$\beta_w = \sqrt{\frac{2 - b_{frp} / b_c}{1 + b_{frp} / b_c}} \tag{1.6d}$$

The performance of their model in evaluating the strength of specimens tested in this study will be presented in Chapter 3.

The results of these studies revealed that anchorage strength can widely vary due to uncertainties associated with material properties, application methods, and testing procedures. Therefore, room for developing reliable anchorage methods, estimation of material parameters, and improvement of anchorage strength models is still wide open.

1.3 OBJECTIVES AND SCOPE

The objective of this study is to investigate the ultimate shear capacity of carbon fiber reinforced polymer (CFRP) laminates bonded to different structural materials which are usually used in typical buildings of Turkey and determine the effects of the parameters:

- material type (low and normal strength concrete, hollow clay tile)
- anchorage type (strip, fan, and embedded types)
- effects of the plaster over the surface

- width of the CFRP laminate
- bond length of the CFRP laminate

At the end of the experimental program, a simple design oriented analytical model derived for the ultimate shear strength of the strip type anchors bonded to concrete and hollow clay tiles with or without plaster over the bonded surface is presented.

Detailed information about test specimens, test setup, testing procedure, instrumentation, material properties, and test results are stated in Chapter 2, analytical model and conclusions are presented in Chapter 3 and Chapter 4, respectively.

CHAPTER 2

EXPERIMENTAL PROGRAM

2.1 INTRODUCTION

In the literature, a number of different test setups were employed to investigate the strength of CFRPs bonded to concrete. A recent survey of Yuan et al. [18] classified these setups into three basic groups such as single shear, double shear, and beam tests which are presented in Figure 2.1. None of these studies were conducted using low strength concrete or HCT masonry units. Furthermore, the presence of the plaster on concrete or HCT setup units was not investigated in these studies. The results of experiments, conducted to fill this gap in the literature, are presented in this chapter.

It can be observed that double shear tests are comparably easier to utilize and they do not require the use of any special anchorages to concrete blocks. On the other hand, beam tests impose both shear and peeling stresses at the FRP concrete interface. Hence, they are generally employed to investigate failure modes of FRPs bonded to concrete beams. Since the objective of this study is to investigate the shear strength of CFRPs bonded to plastered infill wall surfaces and reinforced concrete beams, double shear test setup is employed. In this way, it was possible to conduct a large number of tests in a systematical way due to the ease of specimen preparation and testing.

In this chapter, details of test setup, test specimens, material properties, instrumentation, and experimental results are described in detail.

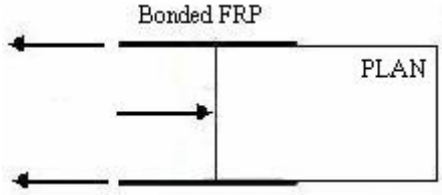

(a) Double Shear Test

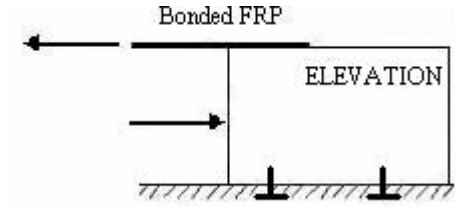

(b) Single Shear Test

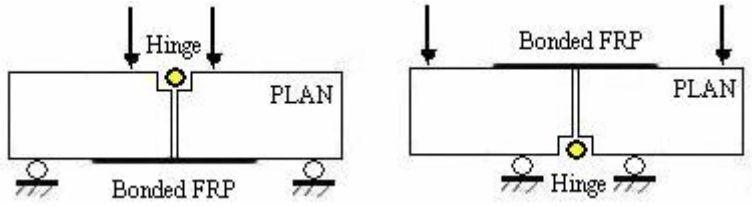

(c) Beam Tests

Figure 2.1 Classification of Bond Tests

2.2 MATERIAL PROPERTIES

2.2.1 Carbon Fiber Reinforced Polymer (CFRPs)

In this study, a single type commercially available unidirectional carbon fiber reinforced polymer (CFRP) laminate was used. CFRP composites used in this study were composed of an epoxy based matrix and CFRP laminates. Epoxy resin adhesive in the matrix was also composed of two components that require mixing before impregnation of CFRPs. Mechanical properties of the carbon fiber reinforced laminates reported by the manufacturer and the epoxy used in the experimental program are given in Table 2.1 and Table 2.2, respectively.

Table 2.1 Mechanical Properties of Carbon Fiber Reinforced Polymer

Property	Amount	Unit
Unit Weight	0.300	kg/mm^2
Effective Thickness	0.165	mm
Characteristic Tensile Strength	3430	MPa
Characteristic Elastic Modulus	230000	MPa
Ultimate Strain	0.015	mm/mm

Table 2.2 Mechanical Properties of Adhesive

Property	Amount	Unit
Compressive Strength	>80	MPa
Direct Tensile Strength	>50	MPa
Flexural Tensile Strength	>120	MPa
Elastic Modulus	>3000	MPa
Ultimate Strain	>0.025	mm/mm

Due to impregnation of CFRPs with adhesive, a new composite material is formed with different material properties from both components. Therefore, properties and stress-strain behavior of the new composite material were obtained conducting flat coupon tests. These tests were conducted in METU-Material and Construction Laboratory, as part of this study.

For the coupon tests, three strips of CFRP with the dimensions of 450 mm x 25 mm were prepared. Thicknesses of these three CFRP strips were 1, 1.05 and 1 mm, respectively. Steel plates with the dimensions of 150 mm x 50 mm x 3 mm were fixed to the heads of the CFRP strips using high strength epoxy. Steel headings helped to fix the strip to the loading machine and avoid the slip at the head of the loading machine. A photograph of the coupon test is given in Figure 2.2 and experimentally obtained stress-strain relationship of three CFRP strips are presented in Figure 2.3.

(a) During Loading

(a) Failure of the CFRP

Figure 2.2 Pictures of the Coupon Tests

In the coupon tests, strain values obtained using strain gauges that were located at the center line of the CFRP strip. A dial gage was also used between the heading steel plates to verify the strain gage readings. Ultimate tensile strengths of the coupon tests 1, 2 and 3 were 431.64 MPa, 541.51 MPa, and 384.55 MPa, respectively. Maximum strain in the test was 0.0085 mm/mm. Failures of the tests 1 and 3 occurred (at relatively low strengths) due to stress concentration near the steel heading of the CFRP strips. On average, modulus of elasticity of the CFRP composite was found to be about 61000 MPa. Previous flat coupon tests conducted using the same material resulted in similar strength values when compared to those obtained from Coupon Test 2 [10].

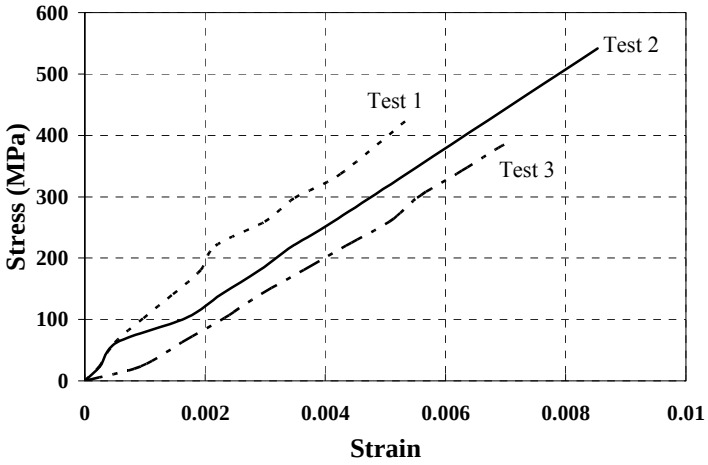

Figure 2.3 Stress-Strain Curves of the Coupon Tests

2.2.2 Concrete

In this study, concrete prisms with the dimension of 300 mm x 200 mm x 200 mm were used (Figure 2.4). Two different concrete strength, low and normal strength concrete, were used in the experimental program. The mixed proportions for both low and normal strength concrete prisms are given in Table 2.3. For each strength group, two sets of specimens were prepared.

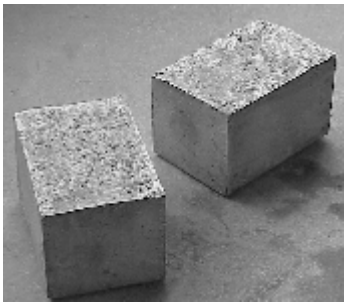

Figure 2.4 Picture of Concrete Specimens

Cylinders of 150 mm x 300 mm were also prepared for each concrete mixture to determine the compressive strength of the prisms. Concrete cylinder compressive strength tests conducted in METU-Structural Mechanics

Laboratory at 28th day of the concrete casting. Concrete cylinder compressive strength of the low and normal strength concretes are given in Table 2.4.

Table 2.3 Mixture Proportions of Low and Normal Strength Concrete

Material	**Low Strength Concrete**		**Normal Strength Concrete**	
	Mass (kg)	Proportion of Weight (%)	Mass (kg)	Proportion of Weight (%)
Cement (32.5 MPa)	21.42	11.9	32.94	18.3
0-3 mm Aggregate	34.38	19.1	54.90	30.5
3-7 mm Aggregate	68.40	38.0	49.50	27.5
7-15 mm Aggregate	36.00	20.0	27.90	15.5
Water	19.80	11.0	14.76	8.2
Total	180	100	180	100

Table 2.4 Cylinder Compressive Strengths of Concrete

Specimen	**28th day f_c (MPa)**
1st set of Low Strength Concrete	10.6
2nd set of Low Strength Concrete	17.8
1st set of Normal Strength Concrete	31.0
2nd set of Normal Strength Concrete	29.8

2.2.3 Hollow Clay Tile (HCT)

In the experimental study, HCTs, named as high strength tile in construction literature, with the dimensions of 280 mm x 180 mm x 130 mm were used and a photograph of the tile is shown in Figure 2.5.

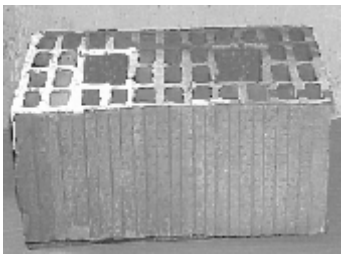

Figure 2.5 Picture of the HCT

HCTs loaded parallel to cores in the METU-Structural Mechanics Laboratory to determine its compressive strength. The compressive strength of the HCT was found as 6 MPa and 11 MPa considering the gross and net areas (~55% of gross area), respectively.

2.2.4 Plaster

An important parameter in the experimental program was to investigate the effect of the plaster layer on concrete and HCT surfaces. The mix proportion for the plaster is given in Table 2.5.

Table 2.5 Mixture Proportions of Plaster

Material	Proportion of Weight (%)
Cement (32.5 MPa)	12.5
Sand	62.5
Lime	8.5
Water	16.5
Total	100

Cylinders of 75 mm x 150 mm were prepared for each plaster mixture to determine the compressive strengths. These strength values and the thickness of the plaster over the bonding surface are given in Table 2.7 and Table 2.8 for the strip and embedded type anchors, respectively. Average strength of the plaster calculated was about 4.9 MPa, which is similar to plaster used generally in Turkish construction practice.

2.3 EXPERIMENTAL SETUP

In the experimental program, 60 tests (three of these tests conducted to determine strain profile along the bond length) were performed. 42 of these experiments were conducted on concrete specimens given in Section 2.2.2,

whereas the remaining 18 tests were performed on HCT specimens given in Section 2.2.3.

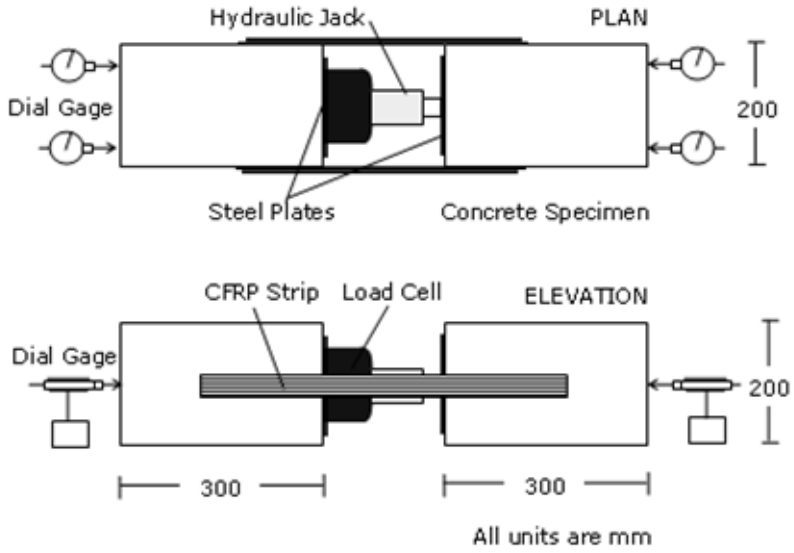

Figure 2.6 Experimental Setup

Plan and elevation views of the test setup used in the experiments are presented in Figure 2.6.

The experimental setup consisted of two identical concrete or HCT prisms and two sheets of CFRP laminate bonded horizontally at the center line of the system. Load was applied using a hydraulic jack through the centerline of two prisms, such that two blocks are pushed against each other while imposing shear stresses at the CFRP-block interfaces. Special attention was given to eliminate any possible eccentricities on CFRP laminates that could cause premature failure. To achieve this, positioning of the hydraulic jack along the centerline was performed with special care for each specimen. Two steel plates with the dimensions of 280 mm x 180 mm x 5 mm were located on loading faces of the specimens to avoid local failure of the specimens and to distribute stresses uniformly.

Pictures of the double shear test specimens with concrete and HCT units are presented in Figure 2.7.

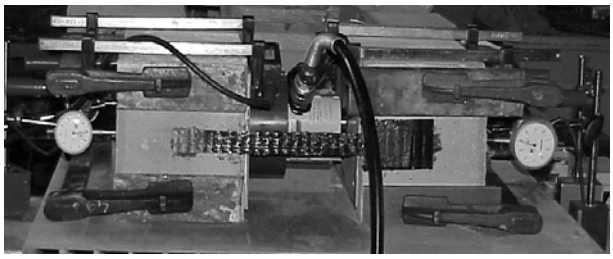

(a) Concrete Specimen

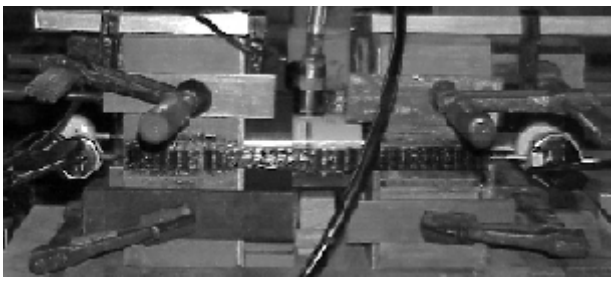

(b) HCT Specimen

Figure 2.7 Pictures of the Experimental Setup

2.4 TEST SPECIMENS

A total of 57 tests in thirteen groups, which were presented in Table 2.6, were conducted in the experimental program (excluding 3 specimens that were prepared to obtain strain distribution on CFRP) to investigate the effects of the strength of the concrete prisms or HCTs (f_c), presence of plaster, CFRP width (b_{frp}), CFRP bond length (L_{frp}), embedment depth (d_{frp}), spread angle of fan anchors (α), and anchor type. Test program and parameters used in the experiments of this study are tabulated in Table 2.6.

Table 2.6 Test Program and Specimens

Type	Group ID	Specimen ID	Specimen Parameters								
			f_c (MPa)	L_{frp} (mm)	b_{frp} (mm)	d_{frp} (mm)	s (mm)	α	r_1 (mm)	r_2 (mm)	Plaster
Strip Type Anchorages	Group 1	LCS-1	10.6	75	25						-
		LCS-2	10.6	100	25						-
		LCS-3	10.6	125	25						-
		LCS-4	10.6	150	25						-
		LCS-5	10.6	75	50						-
		LCS-6	10.6	100	50						-
		LCS-7	10.6	125	50						-
		LCS-8	10.6	150	50						-
	Group 2	NCS-1	31.0	50	25						-
		NCS-2	31.0	100	25						-
		NCS-3	31.0	125	25						-
		NCS-4	31.0	150	25						-
		NCS-5	31.0	50	50						-
		NCS-6	31.0	100	50						-
		NCS-7	31.0	125	50						-
		NCS-8	31.0	150	50						-
	Group 3	TS-1	6.0	50	25						-
		TS-2	6.0	75	25						-
		TS-3	6.0	100	25						-
		TS-4	6.0	125	25						-
		TS-5	6.0	50	50						-
		TS-6	6.0	75	50						-
		TS-7	6.0	100	50						-
		TS-8	6.0	125	50						-
	Group 4	LCSP-1	10.6	75	25						+
		LCSP-2	10.6	100	25						+
		LCSP-3	10.6	125	25						+
		LCSP-4	10.6	150	25						+
	Group 5	NCSP-1	31.0	50	25						+
		NCSP-2	31.0	100	25						+
		NCSP-3	31.0	125	25						+
		NCSP-4	31.0	150	25						+
	Group 6	TSP-1	6.0	50	25						+
		TSP-2	6.0	75	25						+
		TSP-3	6.0	100	25						+
		TSP-4	6.0	125	25						+
Embedded Type Anchorages	Group 7	LCE-1	17.8	50	25	25			7.5	5	-
		LCE-2	17.8	50	25	50			7.5	5	-
		LCE-3	17.8	50	25	75			7.5	5	-
	Group 8	NCE-1	29.8	50	25	25			7.5	5	-
		NCE-2	29.8	50	25	50			7.5	5	-
		NCE-3	29.8	50	25	75			7.5	5	-
	Group 9	TE-1	6.0	120	25	130	60				-
		TE-2	6.0	120	25	130	40-80				-
		TE-3	6.0	120	25	130	30				-
	Group 10	LCEP-1	17.8	50	25	25			7.5	5	+
		LCEP-2	17.8	50	25	50			7.5	5	+
		NCEP-1	29.8	50	25	25			7.5	5	+
	Group 11	TEP-1	6.0	120	25	130	60				+
		TEP-2	6.0	120	25	130	40-80				+
		TEP-3	6.0	120	25	130	30				+
Fan Type Anchorages	Group 12	LCF-1	17.8	50	25			30°			-
		LCF-2	17.8	75	25			30°			-
		LCF-3	17.8	100	25			30°			-
	Group 13	LCF-4	17.8	50	25			60°			-
		LCF-5	17.8	75	25			60°			-
		LCF-6	17.8	100	25			60°			-

NOTES: +: present -: absent

L_{frp}: CFRP bond length, b_{frp}: CFRP width, α: spread angle, r_1 : hole radius, r_2 : hole edge curvature, d_{frp}: CFRP embedment depth, s: displacements of dowels of the HCT specimens from loaded edge

2.4.1 Strip Type Anchors

Schematic of surface bonding of CFRPs to blocks, named hereafter as strip type anchor, is presented in Figure 2.8. Specimens without plaster in the first group were low strength concrete prisms with different bond lengths. Second group of specimens were repetition of first group, the only difference being the strength of concrete prisms. For the first two group tests, rectangular CFRP patches were bonded to ensure that failure occurred on the monitored anchor without any patches. In this way, it was possible to attach strain gauges economically on the anchor that would eventually fail with debonding. These extra CFRP strips were not used in experiments of tile specimens and specimens with plaster. Preliminary tests showed that use of additional CFRP patches adversely affects the failure modes and strength of the HCT specimens and specimens with plaster finish. When these CFRP patches were used on plastered blocks, failure occurs due to complete detachment of the plaster from concrete surface along the patch. Hence, they no longer serve as a way of forcing the failure to the monitored anchorage.

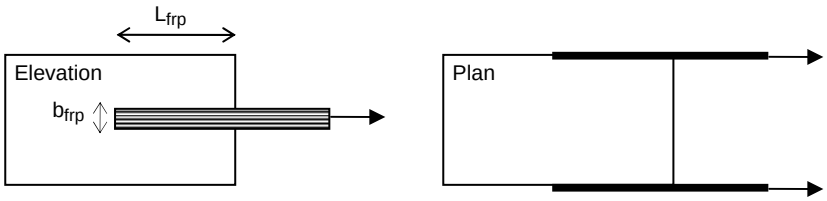

(a) Drawing of the Strip Type Anchorages

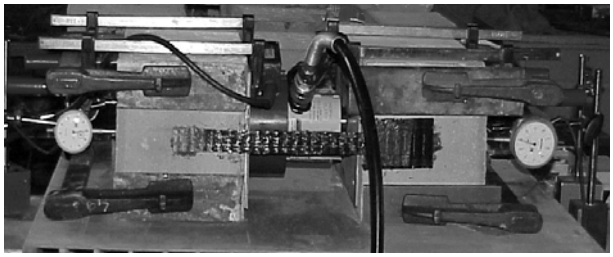

(b) Photograph of the Strip Type Anchorages bonded to concrete

Figure 2.8 Strip Type Anchorage

The third group of the tests consisted of HCTs without plaster. CFRP width (b_{frp}) and CFRP bond length (L_{frp}) were test variables in this group. These two variables were selected same as the first two group parameters to make a comparison between low strength concrete, normal strength concrete, and HCTs.

Fourth, fifth, and sixth group of specimens with plaster employed test variables similar to those used in Group 1, 2, and 3. Presence of plaster and CFRP bond length (L_{frp}) were the parameters under investigation.

2.4.2 Embedded Type Anchors

Second type of anchors in the experimental program was the embedded type anchor and is presented in Figure 2.9 for concrete specimens and in Figure 2.10 for tile specimen units. Three tests for each group of blocks (low strength concrete, normal strength concrete, and HCT specimens) were performed without plaster on the bonding surface and were named respectively as seventh, eighth, and ninth groups.

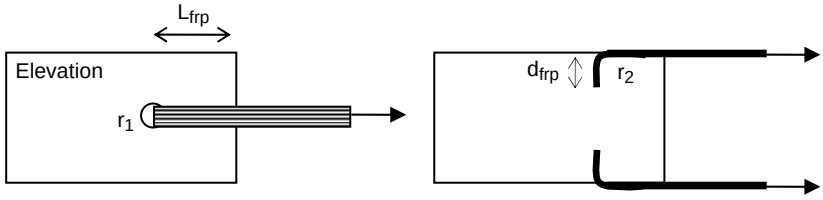

(a) Drawing of the Embedded Type Anchorages

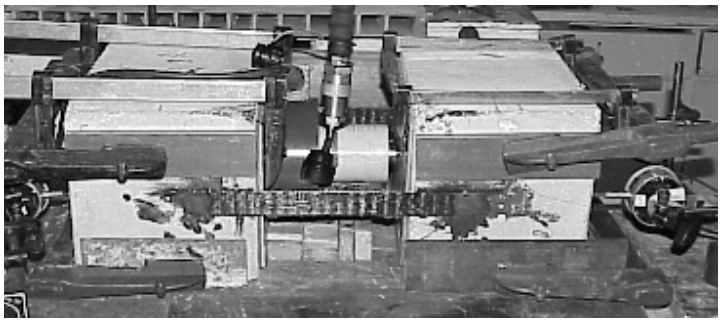

(b) Photograph of the Embedded Type Anchorages

Figure 2.9 Embedded Type Anchors Bonded to Concrete

For embedded type anchors, different details were used for concrete and HCT units. For concrete specimens in Group 7 and 8, free end of the CFRP was embedded in a hole drilled in concrete prisms as presented in Figure 2.9 (in the tests of concrete specimens, hole was filled with epoxy based matrix after bonding of CFRP). Parameters namely bond length (L_{frp} = 50 mm) and CFRP width (b_{frp} =25 mm) were constant and embedment depth (d_{frp}) was the only test variable in the tests of concrete block units.

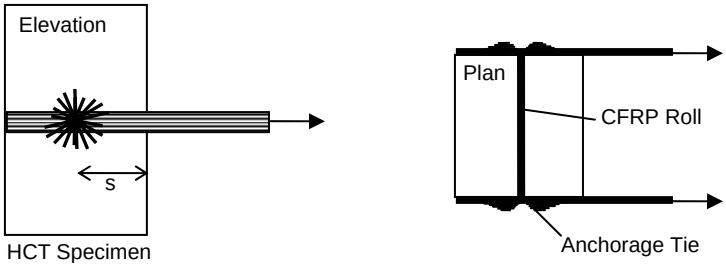

(a) Drawing of the Embedded Type Anchorages

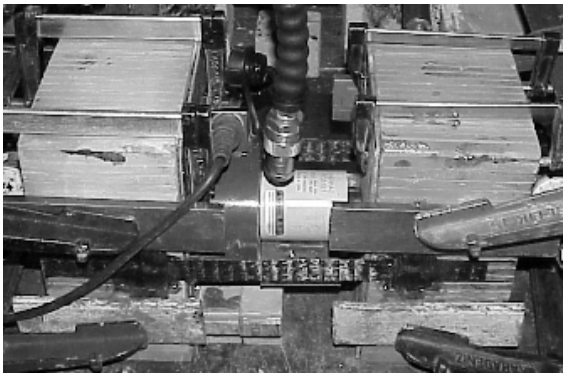

(b) Photograph of the Embedded Type Anchorages

Figure 2.10 Embedded Type Anchors Bonded to HCT

For hollow clay tile specimens of Group 9, special anchor dowels which are presented in Figure 2.10 were prepared by rolling CFRP sheets around a steel wire and impregnating them into epoxy. These CFRP dowels were then passed through the predrilled holes and fanned out on the CFRP strips. For tests on HCT specimens with CFRP dowels, one and two dowel arrangements were used. Specimen TE-1 had one CFRP dowel located 60 mm away from the

loaded side, whereas specimen TE-3 had one CFRP dowel located 30 mm away from the loaded side. Specimen TE-2 had two CFRP anchor dowels located 40 mm and 80 mm away from the free end, respectively.

Tests of Group 10 and 11, consisted of concrete and HCT units, were performed to obtain the behavior of the plaster finished specimens. For embedded type anchors, the provided embedment for concrete specimens or CFRP dowels for hollow clay tiles is used to observe the enhancement of bond strength for CFRP-adherent interface of specimens with plaster or without plaster.

2.4.3 Fan Type Anchors

Fan type is the last anchorage type in the experimental program which is composed of Group 12 and 13 specimens with only low strength concrete prisms. Parameters in the tests were the CFRP bond length (L_{frp}) and the spread angle (α) where CFRP width (b_{frp}=25 mm) was constant. Fan type anchorage figures are presented in Figure 2.11.

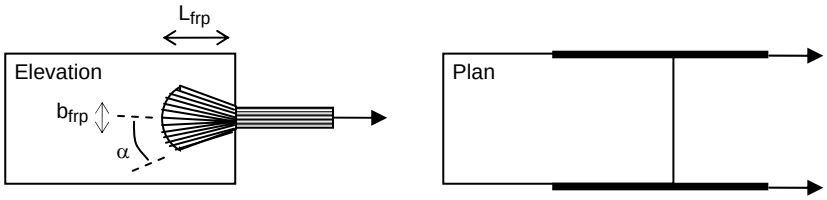

(a) Drawing of the Fan Type Anchorages

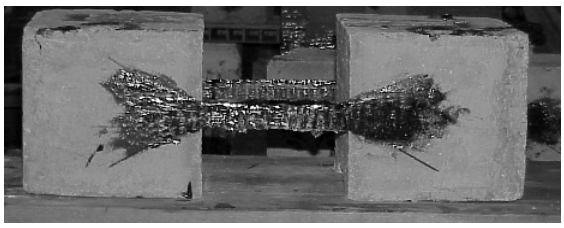

(b) Photograph of the Fan Type Anchorages

Figure 2.11 Fan Type Anchorage

2.5 CFRP APPLICATION AND DETAILS

Prior to application of the CFRPs, surfaces of concrete, HCT blocks, or plaster finished surfaces were cleaned from dust by air-blowing. Then, CFRP sheets, cut to predetermined length and width, were impregnated into epoxy resin and bonded on the sides of the blocks. Wooden plywood sheets covered with plastic nylon were attached and C-clamps were used to keep the CFRP sheets in correct position while curing of the epoxy. After curing, wooden blocks were removed and testing equipment was attached without moving the specimens. All the tests were performed after three days of CFRP application for a uniform amount of curing time.

2.6 INSTRUMENTATION

The data were collected automatically using a computerized data acquisition system which was given in Figure 2.12 with the other instrumentation equipments.

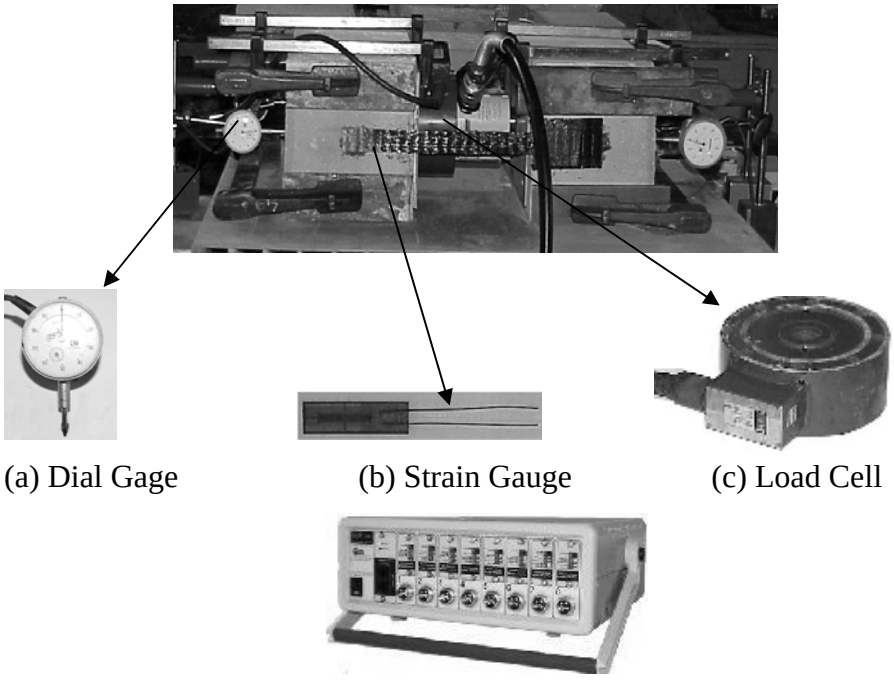

(a) Dial Gage (b) Strain Gauge (c) Load Cell

(d) DAQ System

Figure 2.12 Instrumentation Equipments

Applied load was measured using a 100 kN load cell that was located next to the hydraulic jack in horizontal direction as shown in Figure 2.6. Displacement readings were continuously monitored using 4 dial gages that were located at the outer side of the blocks as shown in Figure 2.6. Strain profile of the strip type anchors was also measured by using 120 Ω strain gauges for 3 concrete specimens without plaster.

2.7 RESULTS AND DISCUSSIONS

Tabulated results of the experimental program including ultimate loads, normalized strength (P_{test}/P_{frp}), and failure modes are given in Table 2.7, Table 2.8, and Table 2.9 for the strip, embedded, and fan type anchors, respectively. As mentioned before, double shear test setup was employed in the experiments. Therefore, P_{test} is equal to half of the total applied load at failure.

Table 2.7 Details of Test Specimens and Test Results of Strip Type Anchors

Test Spec.	Spec. Stren. f_c (MPa)	Spec. Width b_c (mm)	CFRP Width b_{frp} (mm)	CFRP Bond Length L_{frp} (mm)	Plas. Thick. t_p (mm)	Plas. Stren. f_p (MPa)	Failure Load P_{test} (kN)	Failure Mode	P_{test}/P_{frp}
Group 1									
LCS-1	10.6	200	25	75	-	-	3.88	ConDb	0.27
LCS-2	10.6	200	25	100	-	-	4.66	ConDb	0.32
LCS-3	10.6	200	25	125	-	-	5.82	ConDb	0.40
LCS-4	10.6	200	25	150	-	-	5.17	ConDb	0.36
LCS-5	10.6	300	50	75	-	-	4.55	ConDb	0.16
LCS-6	10.6	300	50	100	-	-	8.10	ConDb	0.28
LCS-7	10.6	300	50	125	-	-	9.81	ConDb	0.34
LCS-8	10.6	300	50	150	-	-	9.65	ConDb	0.33
Group 2									
NCS-1	31.0	200	25	50	-	-	4.35	ConDb	0.30
NCS-2	31.0	200	25	100	-	-	5.30	ConDb	0.37
NCS-3	31.0	200	25	125	-	-	4.58	ConDb	0.32
NCS-4	31.0	200	25	150	-	-	6.49	ConDb	0.45
NCS-5	31.0	300	50	50	-	-	7.27	ConDb	0.25
NCS-6	31.0	300	50	100	-	-	9.63	ConDb	0.33
NCS-7	31.0	300	50	125	-	-	12.45	ConDb	0.43
NCS-8	31.0	300	50	150	-	-	10.55	ConDb	0.37

Table 2.7 (continued)

Test Spec.	Spec. Stren. f_c (MPa)	Spec. Width b_c (mm)	CFRP Width b_{frp} (mm)	CFRP Bond Length L_{frp} (mm)	Plas. Thick. t_p (mm)	Plas. Stren. f_p (MPa)	Failure Load P_{test} (kN)	Failure Mode	P_{test}/P_{frp}
Group 3									
TS-1	6.0	280	25	50	-	-	2.84	TileDb	0.20
TS-2	6.0	280	25	75	-	-	4.48	TileDb	0.31
TS-3	6.0	280	25	100	-	-	3.35	TileDb	0.23
TS-4	6.0	280	25	125	-	-	4.06	TileDb	0.28
TS-5	6.0	280	50	50	-	-	3.20	TileDb	0.11
TS-6	6.0	280	50	75	-	-	4.21	TileDb	0.15
TS-7	6.0	280	50	100	-	-	5.90	TileDb	0.20
TS-8	6.0	280	50	125	-	-	5.14	TileDb	0.18
Group 4									
LCSP-1	10.6	200	25	75	13	4.53	1.53	IntDb	0.11
LCSP-2	10.6	200	25	100	13	4.53	2.54	IntDb	0.18
LCSP-3	10.6	200	25	125	11	5.73	2.08	IntDb	0.14
LCSP-4	10.6	200	25	150	11	5.73	2.19	IntDb	0.15
Group 5									
NCSP-1	31.0	200	25	50	12	4.53	1.07	IntDb	0.07
NCSP-2	31.0	200	25	100	11	5.39	2.04	PlaDb	0.14
NCSP-3	31.0	200	25	125	11	5.39	1.93	IntDb	0.13
NCSP-4	31.0	200	25	150	11	5.73	1.26	PlaDb	0.09
Group 6									
TSP-1	6.0	280	25	50	13	4.53	1.46	IntDb	0.10
TSP-2	6.0	280	25	75	13	4.53	1.99	IntDb	0.14
TSP-3	6.0	280	25	100	16	4.76	1.88	IntDb	0.13
TSP-4	6.0	280	25	125	15	4.53	2.69	PlaDb	0.19

Note: P_{frp}: Computed using ultimate strength reported by manufacturer.
ConDb: Debonding in concrete, TileDb: Debonding in HCT, IntDb: Debonding at adhesive-plaster interface, PlaDb: Debonding of plaster from concrete or HCT interface.

Table 2.8 Details of Test Spec. and Test Results of Embedded Type Anchors

Test Spec.	Spec. Stren. f_c (MPa)	Spec. Width b_c (mm)	CFRP Width b_{frp} (mm)	CFRP Bond Leng. L_{frp} (mm)	CFRP Bond Depth d_{frp} (mm)	Plas. Thick t_p (mm)	Plas. Stren. f_p (MPa)	Failure Load P_{test} (kN)	Failure Mode	P_{test}/P_{frp}
Group 7										
LCE-1	17.8	200	25	50	25	-	-	7.91	FrpFail	0.55
LCE-2	17.8	200	25	50	50	-	-	7.07	FrpFail	0.49
LCE-3	17.8	200	25	50	75	-	-	9.36	FrpFail	0.65

Table 2.8 (continued)

Test Spec.	Spec. Stren. f_c (MPa)	Spec. Width b_c (mm)	CFRP Width b_{frp} (mm)	CFRP Bond Leng. L_{frp} (mm)	CFRP Bond Depth d_{frp} (mm)	Plas. Thick t_p (mm)	Plas. Stren. f_p (MPa)	Failure Load P_{test} (kN)	Failure Mode	P_{test}/P_{frp}
Group 8										
NCE-1	29.8	200	25	50	25	-	-	8.45	FrpFail	0.59
NCE-2	29.8	200	25	50	50	-	-	8.20	FrpFail	0.57
NCE-3	29.8	200	25	50	75	-	-	6.14	FrpFail	0.43
Group 9										
TE-1	6.0	280	25	120	130	-	-	6.89	FrpFail	0.48
TE-2	6.0	280	25	120	130	-	-	6.12	TileFail	0.42
TE-3	6.0	280	25	120	130	-	-	5.56	TileFail	0.39
Group 10										
LCEP-1	17.8	200	25	50	25	11	4.76	4.83	FrpFail	0.33
LCEP-2	17.8	200	25	50	50	11	4.76	5.67	FrpFail	0.39
NCEP-1	29.8	200	25	50	25	10	4.76	5.78	FrpFail	0.40
Group 11										
TEP-1	6.0	280	25	120	130	13	4.76	4.46	TileFail	0.31
TEP-2	6.0	280	25	120	130	10	4.76	5.38	TileFail	0.37
TEP-3	6.0	280	25	120	130	14	4.76	4.14	TileFail	0.29

Note: P_{frp}: Computed using ultimate strength reported by manufacturer.
FrpFail: CFRP rupture, TileFail: HCT failure

Table 2.9 Details of Test Specimens and Test Results of Fan Type Anchors

Test Spec.	Spec. Stren. f_c (MPa)	Spec. Width b_c (mm)	CFRP Width b_{frp} (mm)	CFRP Bond Leng. L_{frp} (mm)	Spread Ang. α	Plas. Thick t_p (mm)	Plas. Stren. f_p (MPa)	Failure Load P_{test} (kN)	Failure Mode	P_{test}/P_{frp}
Group 12										
LCF-1	17.8	200	25	50	30°	-	-	4.60	FrpFail	0.32
LCF-2	17.8	200	25	75	30°	-	-	5.33	FrpFail	0.37
LCF-3	17.8	200	25	100	30°	-	-	6.29	FrpFail	0.44
Group 13										
LCF-4	17.8	200	25	50	60°	-	-	3.01	FrpFail	0.21
LCF-5	17.8	200	25	75	60°	-	-	4.71	FrpFail	0.33
LCF-6	17.8	200	25	100	60°	-	-	3.69	FrpFail	0.26

Note: P_{frp}: Computed using ultimate strength reported by manufacturer.
FrpFail: CFRP rupture

2.7.1 Strength and Failure Modes

2.7.1.1 Strip Type Anchors

Results of Group 1 (low strength concrete specimens without plaster finish) tests showed that the corresponding maximum strength was found as 40% and 34% of the uniaxial load carrying capacity of the CFRPs for 25 mm and 50 mm wide strips, respectively. According to the test results, with increasing bonded length, L_{frp}, load carrying capacity increases up to a certain length beyond which no strength enhancement occurs. This length, generally referred as the effective bond length [22], was found to be about 100 mm for a concrete strength of about 10 MPa. Normalized strength variation for different bond lengths and CFRP widths are presented in Figure 2.13. From this group of tests, it was evident that increase in width of the CFRP laminates resulted in a decrease of normalized strength.

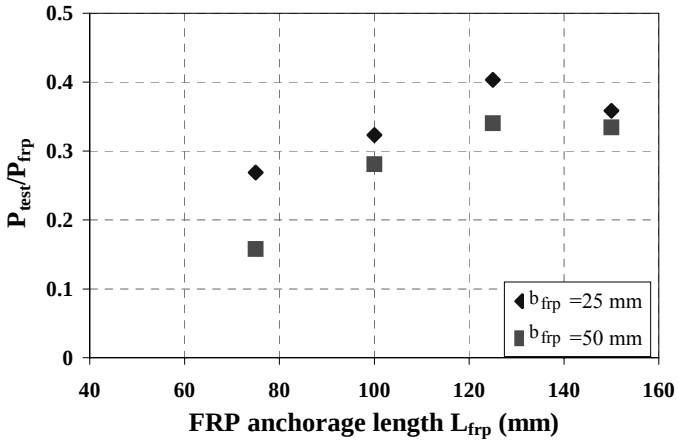

Figure 2.13 Normalized Strength-CFRP Bond Length Behavior of Low Strength Concrete (Group 1) Specimens without Plaster

The failure mode for all specimens in this group was debonding of CFRP from concrete surface. In such a failure, debonding occurred due to failure of concrete at a small distance beneath the bonding surface and a chunk of concrete from loading side of failed block usually remained attached to the

sheet. By decreasing the bond length, length of the failed concrete region and the amount of attached concrete on CFRP increased. Pictures of LCS-1 (L_{frp}=75 mm) and LCS-3 (L_{frp}=125 mm) specimens for 25 mm wide CFRP anchor are shown in Figure 2.14.

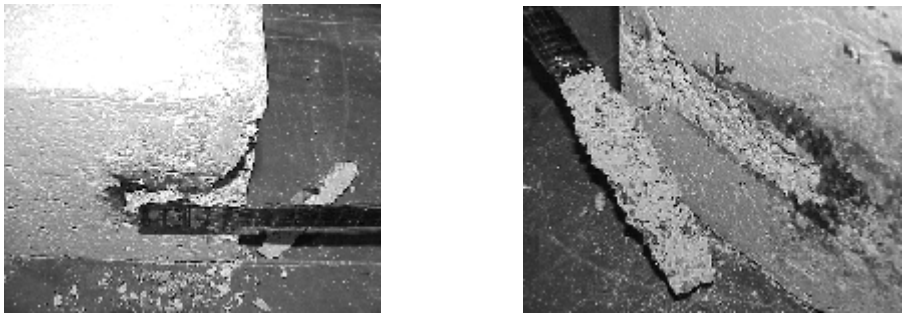

(a) LCS-1 (b) LCS-3

Figure 2.14 Pictures of Debonding in Concrete

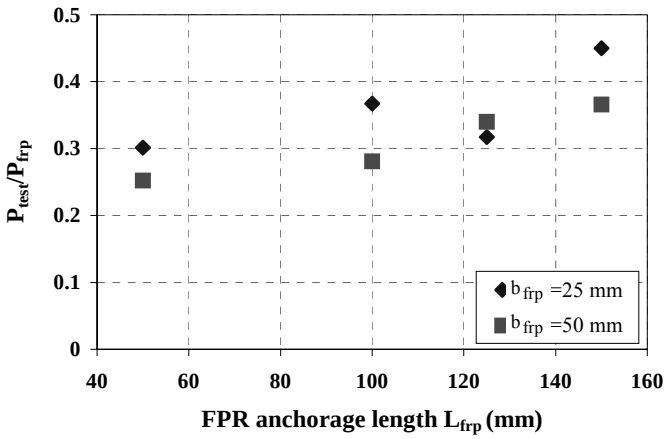

Figure 2.15 Normalized Strength-CFRP Bond Length Behavior of Normal Strength Concrete (Group 2) Specimens without Plaster

For Group 2 (normal strength concrete specimens without plaster finish) tests, similar results to those obtained in Group 1 experiments were observed. The only difference was the higher bond strength, observed as a result of higher concrete strength. Strength of CFRPs bonded to normal strength concrete was about 13% and 20% higher compared to CFRPs bonded to low strength

concrete for CFRP widths of 25 and 50 mm, respectively. According to the normalized strength-CFRP bond length behavior of test results given in Figure 2.15, effective bond length of Group 2 specimens was about 100 to 120 mm. The failure mode of normal strength specimens in Group 2, given in Figure 2.16, was debonding of CFRP from concrete surface, similar to low strength concrete specimens.

(a) NCS-1 (b) NCS-4

Figure 2.16 Pictures of Debonding in Concrete

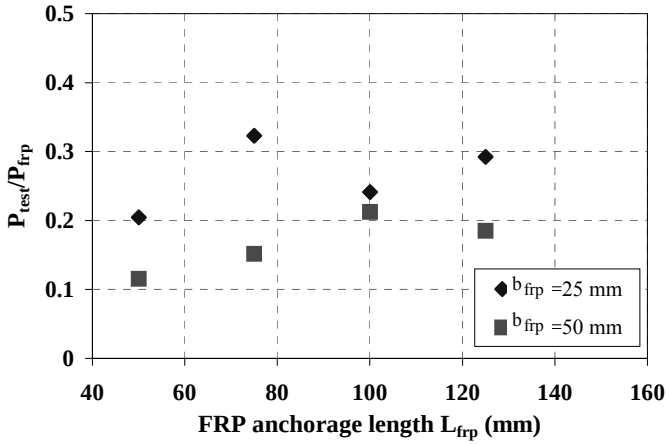

Figure 2.17 Normalized Strength-CFRP Bond Length Behavior of HCT Specimens (Group 3) without Plaster

CFRPs, bonded to HCT specimens without plaster finish in Group 3, had substantially lower strength compared to concrete specimens with similar details. Maximum normalized strength of 31% was obtained for a CFRP width

of 25 mm and 75 mm bond length among all specimens. The effective bond length, which differed due to the discontinuities of the surface of masonry units, was found to be between 75 and 100 mm for masonry blocks according to the normalized strength-CFRP bond length behavior of test results given in Figure 2.17.

For HCTs, debonding process was similar to concrete specimens, but failure occurred in a sudden and brittle manner. All the test specimens in Group 3 exhibited debonding from the HCT surfaces with a small chunk of tile remaining attached on the CFRPs as presented in Figure 2.18 with pictures of TS-3 (L_{frp}=100 mm, b_{frp}=25 mm) and TS-7 (L_{frp}=100 mm, b_{frp}=50 mm).

Results of CFRP bonded to HCT specimens indicated that discontinuities on HCT texture and weak nature of HCTs due to presence of cores are the important factors that can prevent successful bonding of CFRPs, resulting in lower ultimate bond strength. Therefore, texture of masonry units, which are different than that of concrete surfaces, are observed to significantly influence the bond strength of CFRPs.

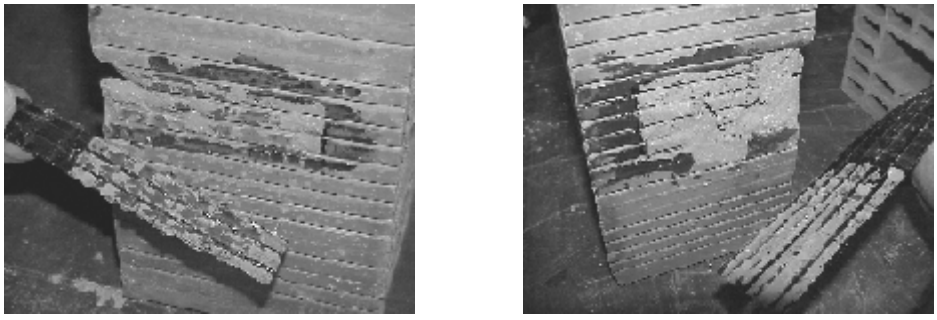

(a) TS-3 (b) TS-7

Figure 2.18 Pictures of Debonding in HCT

Results of test Groups 4, 5, and 6 (plaster finished specimens) showed that the presence of a low strength thin plaster layer (~10 mm) adversely affects the ultimate strength. It can be observed that ultimate strength in the presence of plaster ranged from about 10 to 20 % of the CFRP uniaxial tensile strength.

This was about half of those in the absence of plaster for all three groups of tests. As the strength of plaster was same for all three groups, similar strength values were obtained irrespective of concrete or masonry strength. The only benefit of the presence of plaster, if to mention one, was the elimination of the weak texture on masonry units which was previously observed to result in premature failures. CFRP strength variations for different bond lengths of concrete and HCT plaster finished specimens are presented in Figures 2.19.

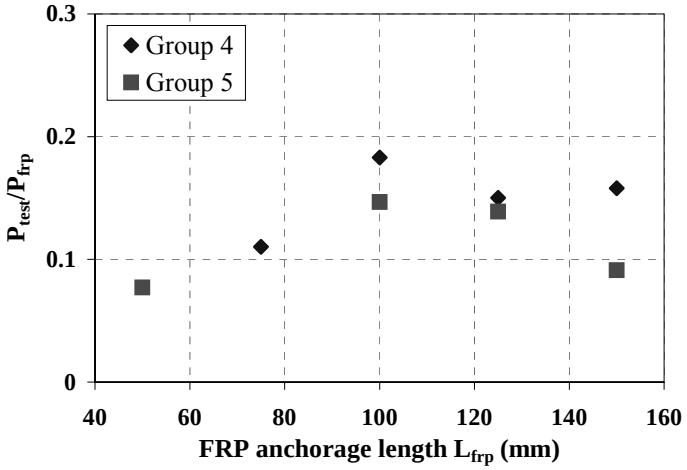

(a) Concrete Specimens

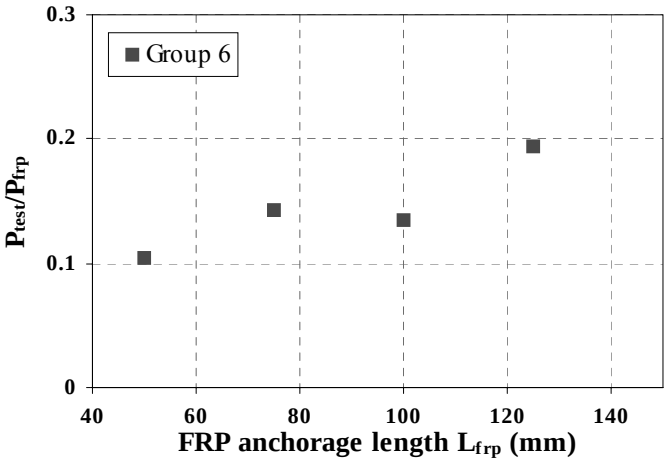

(b) HCT Specimens

Figure 2.19 Normalized Strength-CFRP Bond Length Behavior of Specimens with Plaster

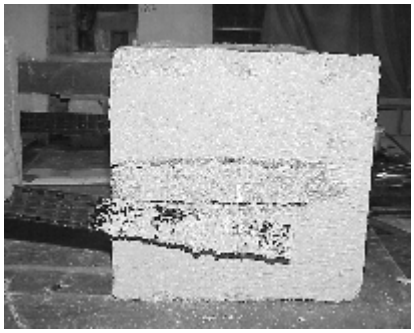

(a) LCSP-4

(b) NCSP-4

(c) NCSP-2

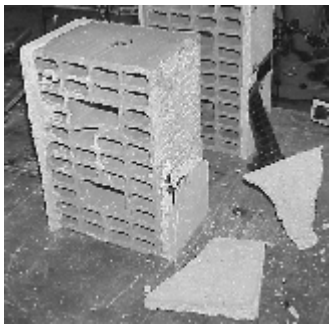

(c) TSP-4

Figure 2.20 Pictures of Failure Modes of Plastered Specimens

For specimens with plaster finish (Groups 4, 5, and 6), two failure modes were observed. The first failure mode was debonding at CFRP-plaster interface for specimens LCSP1, LCSP2, LCSP3, LCSP4, NCSP1, NCSP3, TSP1, TSP2, and TSP3. A typical picture of this failure mode is shown in Figure 2.20(a). Average bond strength of these specimens was 12% of CFRP uniaxial tensile strength. The second failure mode, debonding at plaster-concrete interface, was observed for specimens NCSP-2, NCSP-4, and TSP-4. Bond strength of these specimens varied between 0.09 and 0.19 times CFRP uniaxial tensile strength. For specimen NCSP-4, complete debonding of plaster from specimen surface was observed (Figure 2.20(b)). For specimens, NCSP-2 and TSP-4, failure initiated at plaster-concrete interface and caused partial separation of the plaster finish from surface of specimens, as shown in Figures 2.20(c) and 2.20(d). It can be observed that regardless of the failure modes

(i.e. CFRP-plaster interface or plaster-concrete interface debonding), comparable bond strength values were obtained. Hence, it is possible to say that when a material with low compressive strength is used as the plaster finish, the load carrying capacity of the anchor, dictated by either modes of failure, are similar. Although not common in Turkish construction practice, using normal strength (~30 MPa) mortar for plastering, is expected to result in plaster-concrete interfacial debonding.

2.7.1.2 Embedded Type Anchors

During the tests of strip type CFRP anchors, the ultimate strength of the specimens were lower compared to CFRP load capacity. Therefore, it was decided to use embedded type of anchors with the aim of enhancing ultimate shear strength of system and avoiding the failure of the system due to debonding at low loads.

Results of Group 7 and 8 experiments conducted on embedded type anchors revealed that embedment enabled the strength of CFRPs to be developed up to about 65% of their ultimate strength irrespective of the embedment depth and concrete strength. In presence of plaster (Group 10), strength was three to four times that of the specimens without any special anchors (Groups 4 and 5) and compressive strength of blocks did not affect the ultimate shear capacity of anchorages. It was also observed that presence of plaster reduced the strength by about 30% for specimens with embedded anchors.

It is important to note that it is still not possible to fully utilize the strength of CFRPs due to stress concentrations occurring around smoothened corners. However, considerable strength enhancement was obtained for all cases with the failure mode changing to CFRP rupture which was not a commonly reported failure mode in the literature due to the lack of bond transfer capacity of CFRPs. Failure process of embedded type anchor bonded specimens with or without plaster started with visible cracks at the loading edge of the anchor and continued with debonding of CFRP from loading edge

to hole edge. With fully debonding of the CFRP up to hole edge, embedded section of the anchor started to carry loads transferred from debonded CFRP sheet. Failure usually occurred at the rounded section of CFRP at hole edge due to stress concentrations. Pictures of rupture of CFRP anchor in specimens NCE-3 and plaster finished LCEP-1 are given in Figure 2.21.

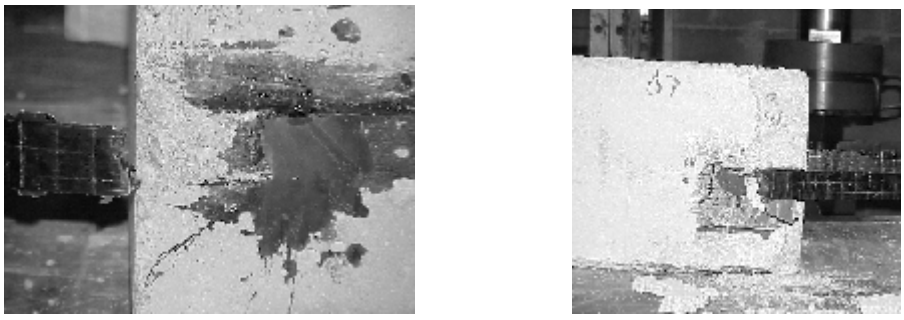

(a) NCE-3 (b) LCEP-1

Figure 2.21 Pictures of CFRP Rupture in Embedded Type Anchorages

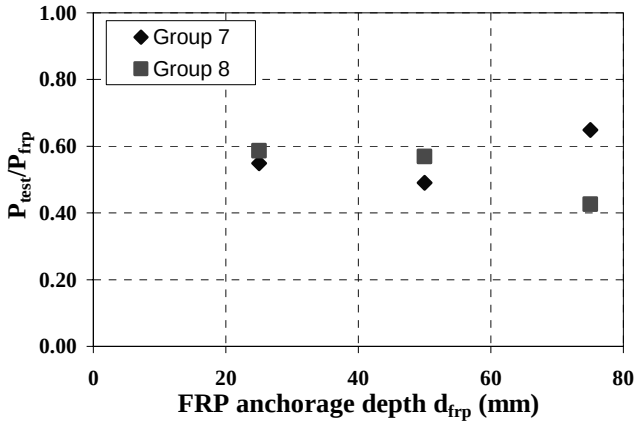

Figure 2.22 Normalized Strength-CFRP Depth Behavior of Concrete Specimens without Plaster

Influence of the embedment depth in specimens was also examined for concrete specimens with embedded anchors. Three different embedment depth d_{frp} =25, 50, and 75 mm were used in tests. Normalized strength-to-anchorage depth behavior of the embedded type anchors bonded to both low and normal strength concrete specimens are given in the Figure 2.22. As presented in the

figure, the effect of concrete strength on the ultimate shear strength of embedded type anchor bonded specimens was limited. Another important result of observations was that the ultimate shear capacity was not affected by the embedment depth.

HCT specimens anchored using embedded CFRP dowels (Group 9) exhibited 50 to 75% higher capacity compared to those without any anchor dowels. This shows that drilled through anchors have beneficial affects to enhance surface bond strength of CFRPs in masonry retrofit applications. Similarly, the bond strength of CFRPs on plastered surfaces increased by a factor of about two when drilled through anchors were used (Group 11). Furthermore, the strength of CFRPs bonded to HCTs equipped with CFRP dowels were comparable to the strength of CFRPs bonded to concrete using embedded anchors. The results of experiments conducted on multiple anchor systems (specimens TE-2 and TEP-2) showed that use of multiple anchors with small spacing has no significant advantage over single CFRP anchors. For all of the specimens in Groups 9 and 11, except specimen TE-1, explosive failure of the HCT units were observed due to the weak nature of HCT as a single unit. Picture of a typical HCT failure is presented in Figure 2.23. However, when CFRPs are applied on masonry walls with continuous HCTs arrangements constructed with mortar joints, single HCT unit failure may not occur and failure can occur as a result of CFRP rupture, as in specimen TE-1.

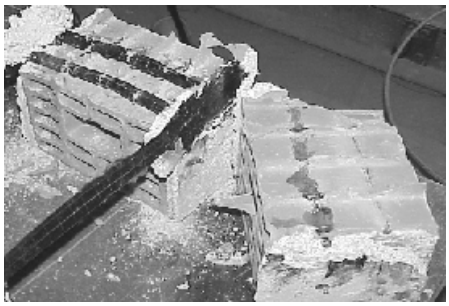

Figure 2.23 Pictures of HCT Failure (TEP-2)

2.7.1.3 Fan Type Anchors

The last two groups of tests (Groups 12 and 13) employed fan type CFRP surface bonding with the aim of enhancing bond strength compared to strip type anchors by increasing the bonded area. During these tests, low strength concrete specimens without plaster were used with constant values of CFRP laminate width which was equal to 25 mm. As presented in Table 2.9, increase in CFRP bond length, which was equal to the fan length at the centerline, increased the ultimate shear capacity, similar to previous tests and observations in the program. Group 12 test results show that when the spread angle, α, was 30 degrees bond capacity increased by about 15% compared to those where spread angle was zero. However, for a spread angle of 60 degrees, capacity decreased by about 30% compared to those where spread angle was 30 degrees. Increase in spread angle resulted in a reduction in strength due to premature failure of CFRPs around spread corners due to stress concentrations.

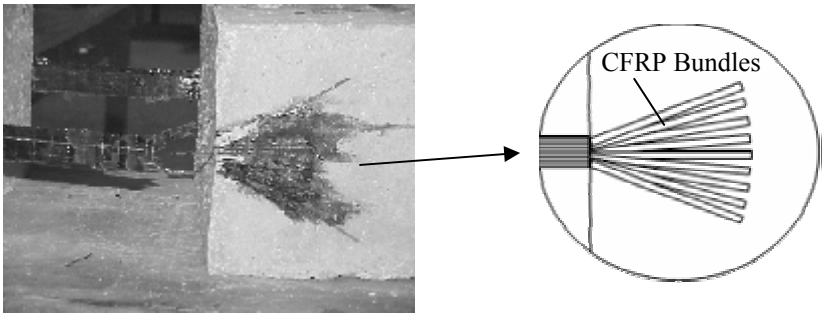

Figure 2.24 Picture of CFRP Rupture (LCF-2)

A picture of LCF-2 specimen is given in Figure 2.24 to show the failure mode in fan type anchors. For the fan type anchors bonded to concrete specimens, CFRP rupture was observed in the tests. Failure occurred at the loading edge of the fan of the anchor due to stress concentration at CFRP.

The normalized shear strength-CFRP bond length behavior of the fan type anchors bonded to low strength concrete specimen without plaster finish are given in Figure 2.25. Results presented in Figure 2.25 show that there is a decrease in the normalized strength upon increasing the bond length from 75 mm to 100 mm for fan anchored specimens with a spread angle of 60°. This decrease can be attributed to forming fan anchors from CFRP sheets with transverse fibers. These transverse fibers were cut carefully and each bundle was then spread out to form a fan (Figure 2.24). However, it was not possible to spread each fiber one by one due to the texture of CFRP sheets. For larger bond lengths, gaps between bundles tended to be larger, resulting in poor transfer of stresses. As a result, the CFRP sheets with transverse fibers can not be practically used to form fans with α larger than 30°. Other types of fibers without any transverse ties seem to be more promising to form fans [11].

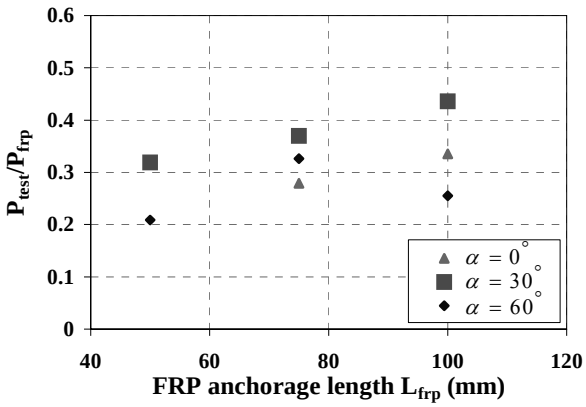

Figure 2.25 Normalized Strength-CFRP Bond Length Behavior of Fan Type Anchorages

2.7.2 Load-Deformation Characteristic

2.7.2.1 Strip Type Anchors

In this section, displacement readings which were obtained with the use of dial gages were used in the curves of the load displacement behavior. These readings called general load-deformation behavior included not only the

anchorage slip but also displacements of the specimens and elastic displacement of the unbonded part of CFRP between the specimens.

General load-displacement relationship of NCS-5 specimen which was commonly seen in this study is given in Figure 2.26. In previous studies [6, 18], it was introduced that load-deformation response is made up of a nonlinear region followed by a small yield plateau. Nonlinear region which occurs due to micro cracks at the anchor-CFRP interface was visible for all the load-displacement curves. Yield plateau, which generally occurs due to progressive debonding of CFRP from concrete (or HCT and plaster) surface was not observed in the experiments of this study. In order to obtain such a response, a displacement-controlled testing is necessary. Since the objective of this study is mainly to investigate the strength properties, a more elaborate setup, consisting of a displacement controller, was not used.

According to Figure 2.26, specimens NCS-5, NCS-6, NCS-7, and NCS-8 behaved in a brittle manner. Furthermore, an increase in the anchor load carrying and displacement capacity was observed with increasing bond length for different concrete uniaxial compressive strength values.

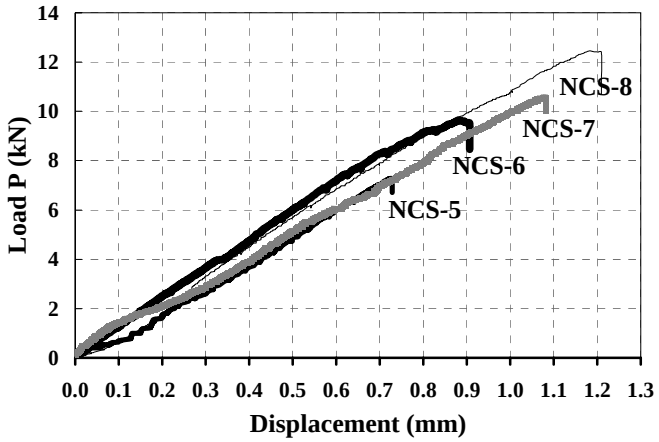

Figure 2.26 Load-Displacement Curves of Spec. NCS-5, NCS-6, NCS-7, and NCS-8

In Figure 2.27, the load-displacement curves of LCS-6 (low strength concrete), NCS-6 (normal strength concrete) and TS-7 (HCT) specimens with the parameters b_{frp}=50 mm and L_{frp}= 100 mm are given. General load-displacement behavior of HCT specimens had a lower stiffness with a smaller ultimate strength. Interestingly, the deformation at failure of tile and low strength specimens were similar. Normal strength concrete specimen had higher shear and displacement capacities compared to LCS-6 and TS-7.

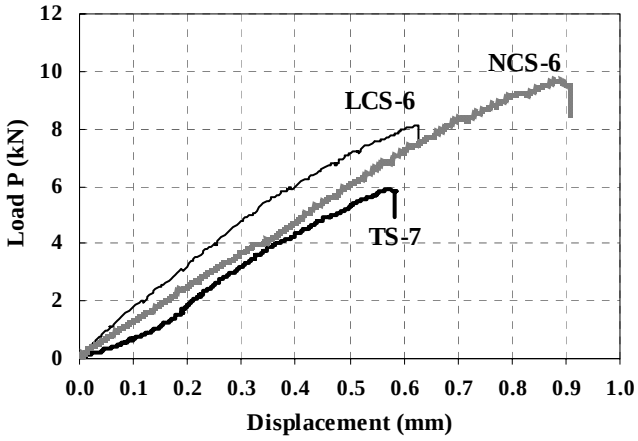

Figure 2.27 Load-Displacement Curves of Specimens LCS-6, NCS-6, and TS-7

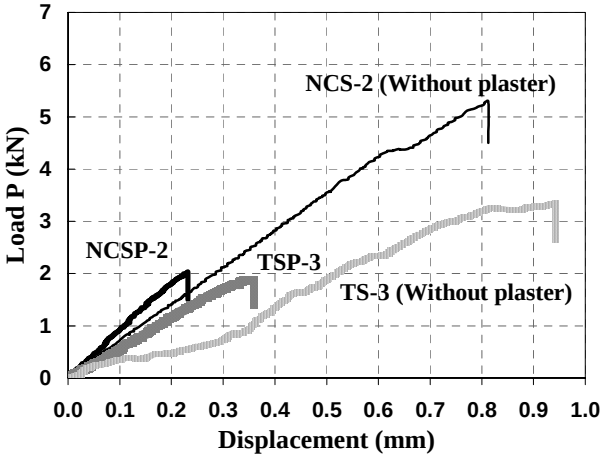

Figure 2.28 Load– Displacement Curves of Specimens NCSP-2, NCS-2, TSP-3, and TS-3

According to the tests on specimens with plaster, it was observed that plaster affected both strength and displacement capacity of the specimens. Load-displacement relationship of normal strength concrete specimens NCSP-2 NCS-2 and HCT specimens TSP-3 and TS-3 with the parameters L_{frp}=100 mm and b_{frp}=25 mm are given in Figure 2.28. According to the presented curves, strength and displacement capacity of strip type anchors bonded to concrete and HCT specimens were lower due to the weakness of the interface between plaster and blocks and poor strength transfer between adhesive and plaster surface. In the tests of specimens without plaster, obtained displacement values were nearly three times of the plaster finished specimens.

2.7.2.2 Embedded Type Anchors

Displacement capacity of the specimens with embedded type anchors were significantly higher compared to the strip type anchors due to full transfer of shear from CFRP to concrete. With the help of the CFRP anchor dowels or embedment, failure of the CFRP anchor at hole edge due to debonding of CFRP from blocks or plaster which started at the loading edge and propagated up to hole edge was reached.

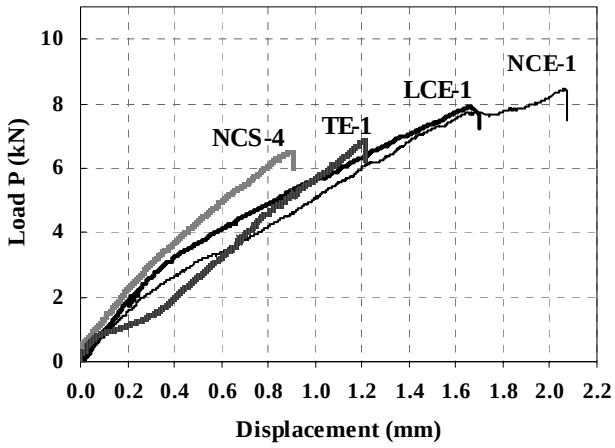

Figure 2.29 Load–Displacement Curves of Spec. LCE-1, NCE-1, TE-1, and NCS-4

The ultimate load capacity and the load-displacement behavior of specimens LCE-1, NCE-1, TE-1 (HCT, one dowel drilled at 60 mm away loading edge), and NCS-4 (strip type anchor bonded to normal strength concrete) with same CFRP sheet width of b_{frp}= 25 mm are given in Figure 2.29. According to the curves, uniaxial compressive strength values of the embedded type anchor bonded specimens slightly affected the slip of the anchor but did not affect the ultimate shear strength significantly. The embedded type anchors enhanced the ultimate shear strength of the system compared to the strip type anchors.

Influence of the embedment depth on the displacement capacity of the embedded type anchor bonded to specimens was also observed for concrete specimens during the experimental program. Figure 2.30 shows the load-displacement curves of Group 7 specimens LCE-1, LCE-2 and LCE-3 (with different embedment depth), which had similar ultimate strength and displacement capacity.

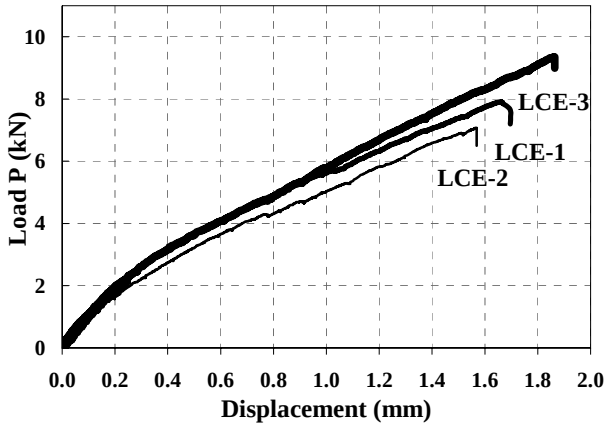

Figure 2.30 Load–Displacement Curves of Spec. LCE-1, LCE-2, and LCE-3

In Figure 2.31, the ultimate load-displacement behavior of specimens TE-1 (HCT specimen without plaster, one CFRP dowel drilled at 60 mm from loading edge), TEP-1 (plaster finished HCT specimen, one CFRP dowel drilled at 60 mm from loading edge), NCE-1 (normal strength concrete without plaster with embedment depth of 25 mm), and NCEP-1 (normal

strength concrete with plaster with embedment depth of 25 mm) are represented to point out the plaster effect. It can be observed that plaster over the bonding surface decreased the ultimate shear strength and increased the displacement capacity of the anchors bonded to concrete or HCT.

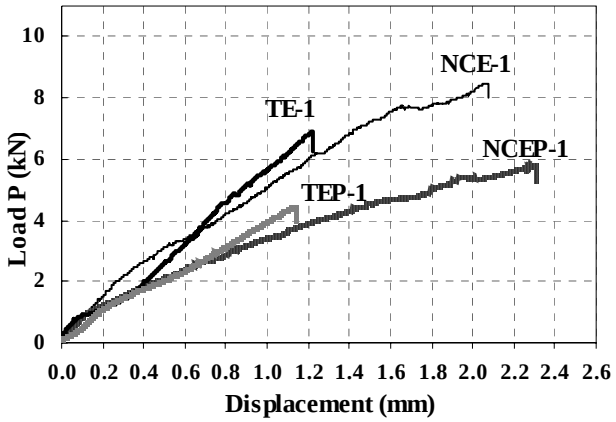

Figure 2.31 Load–Displacement Curves of Specimens TE-1, TEP-1, NCE-1, and NCEP-1

2.7.2.3 Fan Type Anchors

In Figure 2.32, the load-displacement behavior of LCF-1, LCF-2, LCF-3, and LCF-6 specimens are presented to show effects of spread angle and bond length.

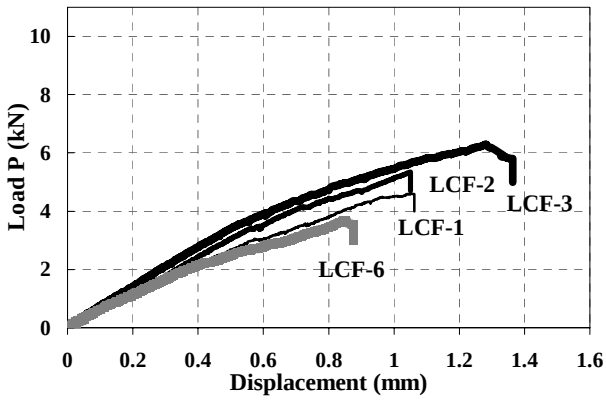

Figure 2.32 Load–Displacement Curves of Specimens LCF-1, LCF-2, LCF-3, and LCF-6

It can be seen that increase in fan angle, due to premature failures, decreased the displacement capacity. On the other hand, increase in bond length of the fan tended to increase the displacement capacity.

2.7.3 Strain Measurements

As part of the study, strain distribution of strip type CFRPs bonded to low strength concrete (17.8 MPa) specimens were investigated for three different anchorage length L_{frp}= 75, 100, and 125 mm and strip width b_{frp}= 50 mm. The ultimate shear strength of these three specimens were 24.2%, 31.3%, and 29.7% of the CFRP uniaxial tensile capacity (6.99 kN, 9.03 kN, and 8.56 kN, respectively).

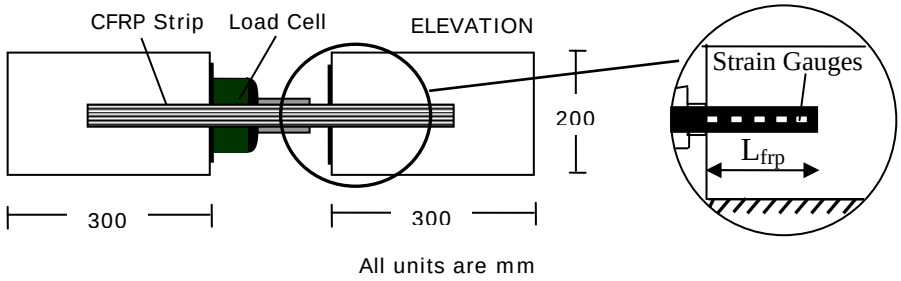

(a) Drawing of Strain Gauge Pasted Specimen

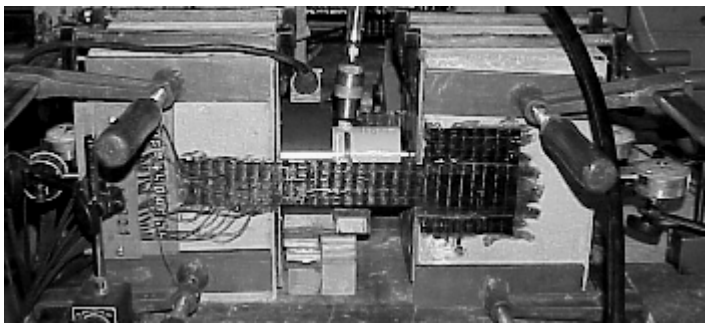

(b) Photograph of Strain Gauge Pasted Specimen

Figure 2.33 Locations of Gauges

Locations of the gages and a photograph of the strain gauged specimen with 100 mm bond length presented in Figure 2.33. All gages in these tests were

bonded parallel to the CFRP loading direction. In Figure 2.34 and Figure 2.35, locations of the gauges on the CFRP strip and strain profile plots are presented. It should be noted that distances of the gauges from the loading edge were measured from the center of the gauge. As presented in these figures, similar ultimate strains at similar locations were obtained.

For the 75 mm strip, which was shorter than the effective length, maximum strain readings were obtained at the same gauge located 32.5 mm away from the loading edge for every load stage. For the 125 mm strip, which was longer than the effective length, maximum strain reading up to 90% of the ultimate load obtained at the point that was 32.5 mm away from the loading edge. After that loading stage, location of the maximum strain shifted to the point that was 57.5 mm away the loading edge due to debonding of CFRP at concrete interface started in the loading edge of the specimen. In Figure 2.35, strain values were zero at the last gauge located at 107.5 mm away from the loading edge which is nearly equal to the effective length for all loading stages.

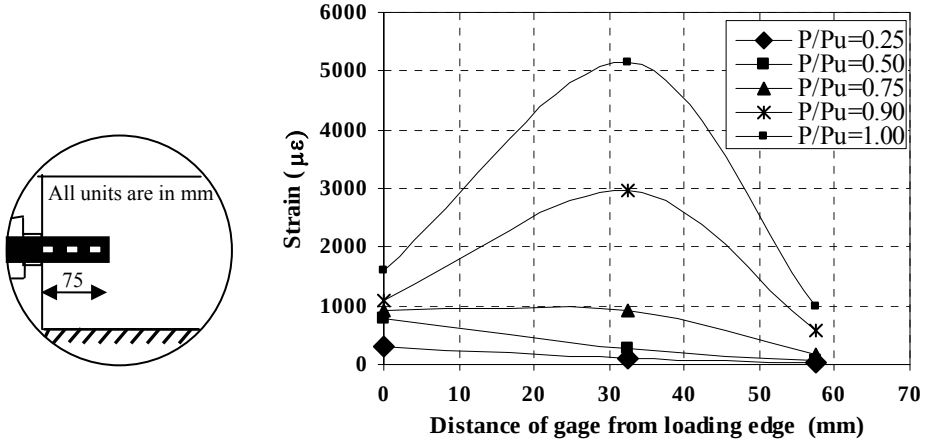

Figure 2.34 Gauge Locations and Strain Reading of CFRP with L_{frp}=75 mm

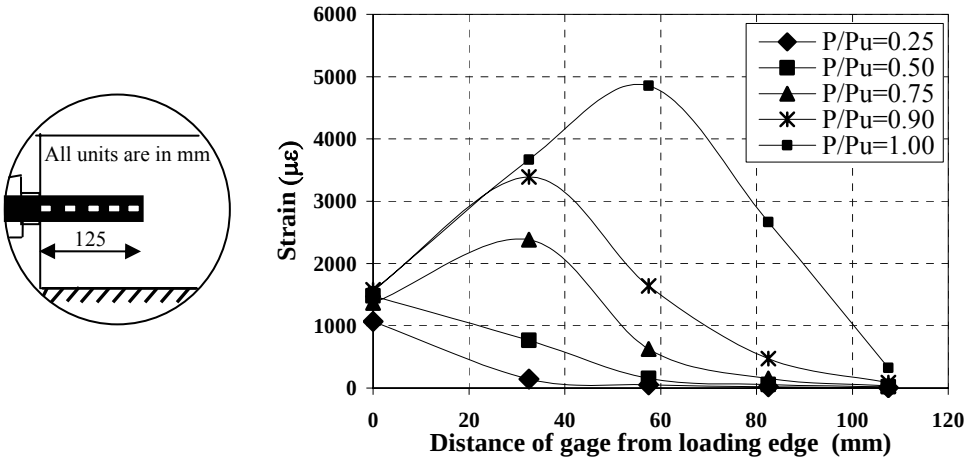

Figure 2.35 Gauge Locations and Strain Reading of CFRP with L_{frp}=125 mm

Locations of the gauges on 100 mm strip bonded to concrete are presented in Figure 2.36. 10 strain gauges were attached on the CFRP strip to observe the strain profile of the strip in both vertical and horizontal directions, but during the test, gauges located at the middle of Sections I-I and II-II failed. Although these failed gauges that prevented full presentation of the strain profile of the strip, sufficient observations and results were obtained with the use of remaining gauges.

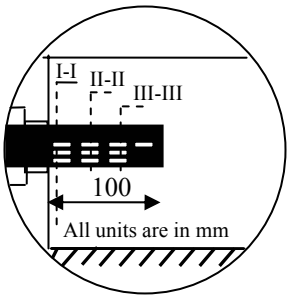

Figure 2.36 Locations of Strain Gauges bonded to CFRP with L_{frp}=100 mm

Strain profiles of the horizontal direction of the strip presented in Figures 2.37 and Figure 2.38. According to the graphs, strains at the outer rows are nearly 50% of the strains at the center row of the strip. Again, similar to the other strain gauges in the program, for the both rows of the 100 mm strip, maximum

strain was observed at the gauges located 32.5 mm away from the loading edge.

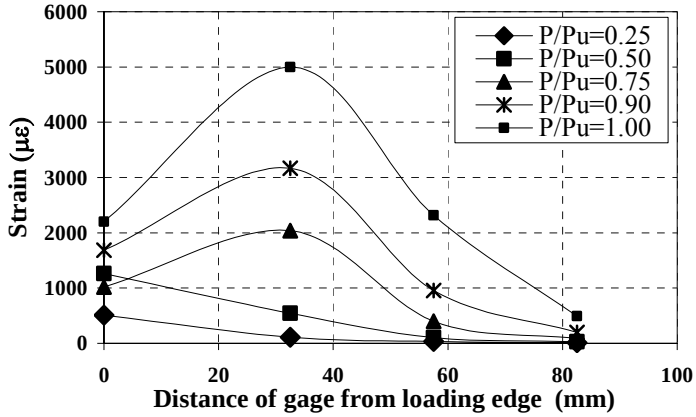

Figure 2.37 Strains of CFRP with L_{frp}=100 mm at centerline

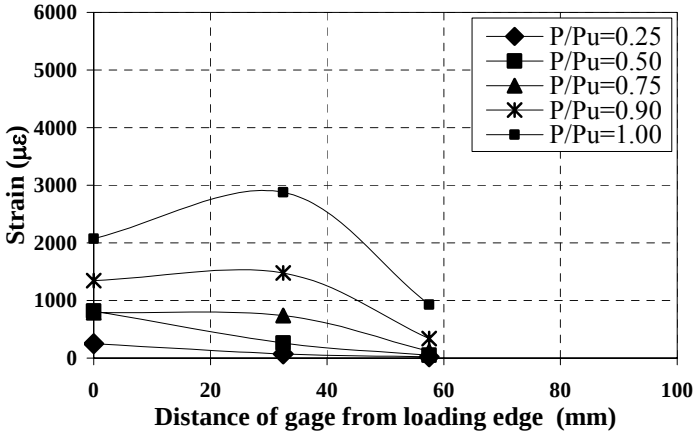

Figure 2.38 Strains of CFRP with L_{frp}=100 mm at outer line of horz. direction

Strain profiles of the vertical direction of the strip are presented in Figures 2.39, 2.40 and 2.41 for Sections I-I, II-II, and III-III, respectively. Strain profiles of Sections I-I, II-II, and III-III show the reduction in the strains. These results showed that, actual strain variation is a three dimensional surface where the strains along the width of the CFRP strips can substantially vary. In general, the largest strains were observed along the centerline and can be accepted as the critical strains.

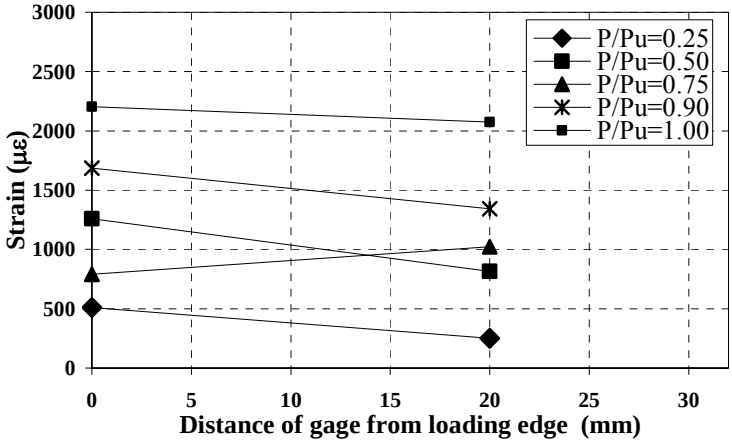

Figure 2.39 Strains of CFRP with L_{frp}=100 mm at Section I-I

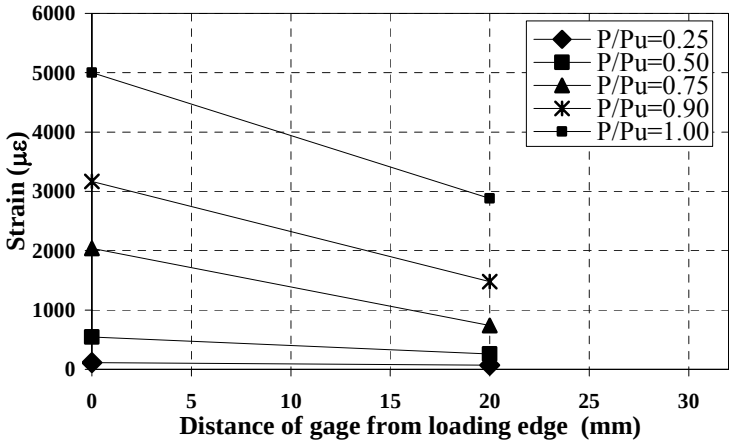

Figure 2.40 Strains of CFRP with L_{frp}=100 mm at Section II-II

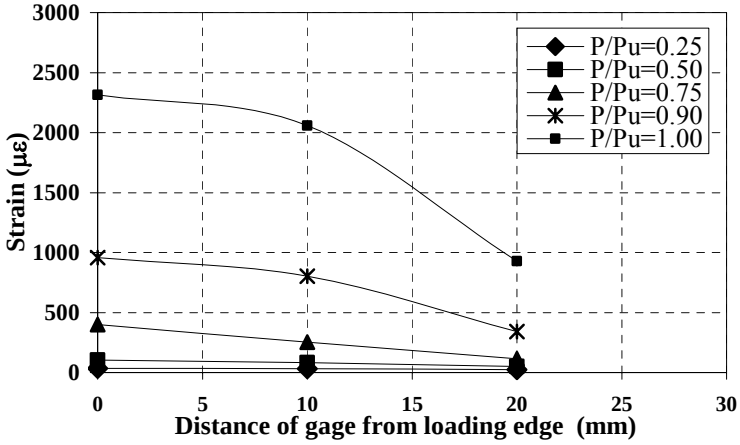

Figure 2.41 Strains of CFRP with L_{frp}=100 mm at Section III-III

CHAPTER 3

ANALYTICAL MODELING

Reliable models are required to estimate the strength of CFRPs bonded to concrete. In this way, it is possible to perform safe CFRP retrofit designs without the need of repeating experiments, similar to those presented in this study, for each specific design case. The details of the developed analytical model are explained in this chapter.

For the strip CFRP anchors, a mathematically rigorous model presented previously for CFRPs bonded to concrete (i.e. with no plaster finish) [18] is extended in this chapter to include the effect of plaster finish. The parameters of this model are calibrated using the results of the experiments presented in Chapter 2. Then, a simplified model that can be used in a design format is proposed. For embedded and fan type anchors, a simple strength model is proposed based on the test results. The accuracy of the developed model is verified by comparing the model estimations to the test results from this study and other experimental studies. Furthermore, the performance of a number of available anchorage strength models are examined using the test results presented in this study.

3.1 STRIP TYPE ANCHORS

3.1.1 Model Assumptions and Derivations

During the derivation process, the following assumptions were made:

- Adherents are homogeneous and linear elastic;
- Bending effects are neglected;
- Normal stresses are uniformly distributed over the cross-section ;

- The thickness and the width of the adherents are constant through the bond line;
- Adhesive and plaster are subjected to shear only.

In Figures 3.1 and 3.2, the deformations and the stresses of the bonded joints are shown together with their free body diagrams. All the notations used are given in the symbols section of this thesis.

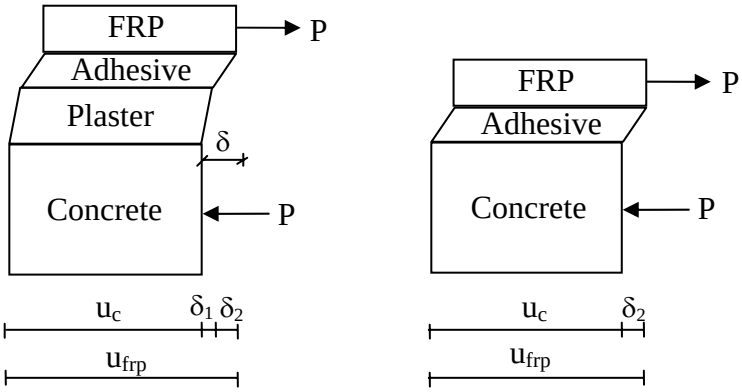

Figure 3.1 Deformations of Specimens with and without Plaster

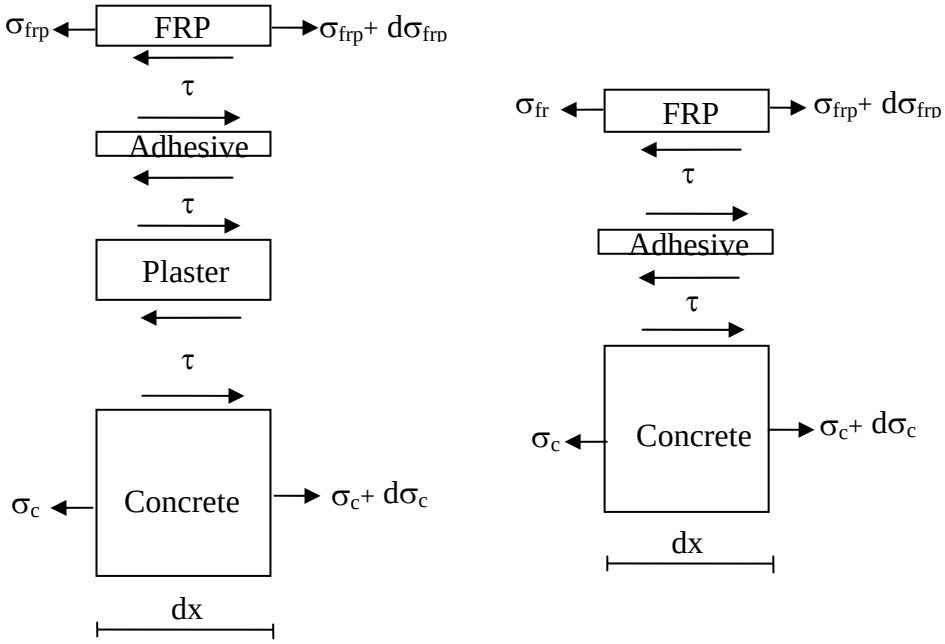

Figure 3.2 Stresses of Specimens with and without Plaster

Considering the plastered concrete section in Figure 3.2, the equations of equilibrium for adherents can be written as:

$$\left(\left(\sigma_{frp} + d\sigma_{frp}\right) - \sigma_{frp}\right) t_{frp}\ b_{frp} - \tau\ b_{frp}\ dx = 0 \tag{3.1a}$$

$$\left(\left(\sigma_c + d\sigma_c\right) - \sigma_c\right) t_c\ b_c + \tau\ b_{frp}\ dx = 0 \tag{3.1b}$$

Eqs.(3.2a) and (3.2b) are obtained from Eqs.(3.1a) and (3.1b).

$$\frac{d\sigma_{frp}}{dx} - \frac{\tau}{t_{frp}} = 0 \tag{3.2a}$$

$$\frac{d\sigma_c}{dx}\frac{b_c}{b_{frp}} + \frac{\tau}{t_c} = 0 \tag{3.2b}$$

Based on the linear elastic assumption of concrete and CFRP, stresses can be written in the form of:

$$\sigma_{frp} = E_{frp}\frac{du_{frp}}{dx} \tag{3.3a}$$

$$\sigma_c = E_c\frac{du_c}{dx} \tag{3.3b}$$

Eq (3.4) is obtained by equating Eqs.(3.2a) and (3.2b):

$$-\frac{d\sigma_{frp}}{dx}\frac{t_{frp}\ b_{frp}}{t_c\ b_c} = \frac{d\sigma_c}{dx} \tag{3.4}$$

The total slip deformation between adherents, δ, is defined in Figure 3.1:

$$\delta = u_{frp} - u_c \tag{3.5}$$

Differentiating both sides twice:

$$\frac{d^2\delta}{dx^2} = \frac{d^2u_{frp}}{dx^2} - \frac{d^2u_c}{dx^2} \tag{3.6}$$

Furthermore, differentiating Eqs.(3.3a) and (3.3b) and substituting in Eq.(3.6), Eq.(3.7) is obtained:

$$\frac{d^2\delta}{dx^2} = \frac{1}{E_{frp}}\frac{d\sigma_{frp}}{dx} - \frac{1}{E_c}\frac{d\sigma_c}{dx} \tag{3.7}$$

Eq.(3.8) is obtained by substituting Eq.(3.4) in Eq.(3.7).

$$\frac{d^2\delta}{dx^2} = \frac{d\sigma_{frp}}{dx}\left(\frac{1}{E_{frp}} + \frac{t_{frp}b_{frp}}{E_c t_c b_c}\right) \tag{3.8}$$

The governing differential equation of the problem is obtained by substituting Eq.(3.2a) in Eq.(3.8):

$$\frac{d^2\delta}{dx^2} = \tau\left(\frac{1}{E_{frp}t_{frp}} + \frac{b_{frp}}{E_c t_c b_c}\right) \tag{3.9}$$

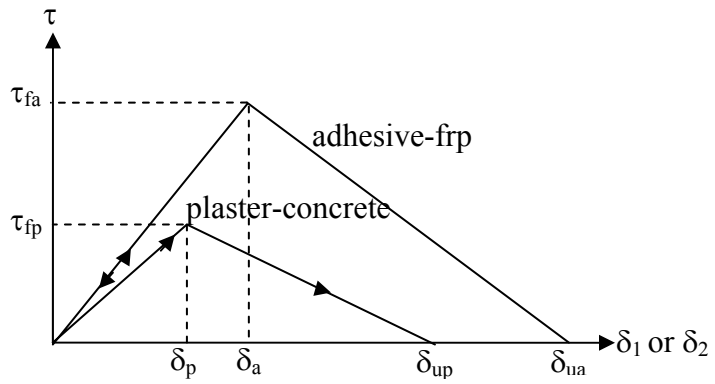

Figure 3.3 τ-δ Relationships of Plaster-Concrete and Adhesive-CFRP Interfaces (Exact Model)

Derivation of the ultimate shear strength formulas of exact and approximate models for plaster finished specimens are presented in Appendix A. The ultimate shear strength of anchors using a linear ascending-descending interface behavior (Figure 3.3), named hereafter as the “exact solution” is:

$$P_u = \frac{\tau_{fp} b_{frp}}{\lambda_2} \frac{\delta_{up}}{\delta_{up} - \delta_p} \sin(\lambda_2 a) \tag{3.10}$$

where a needs to be solved from Eq.(3.11). In Eq.(3.10), τ_{fp} is the shear strength of the plastered layer, b_{frp} is the CFRP width, and δ_{up} and δ_p are the slip displacements as shown in Figure 3.3.

$$\tanh(\lambda_1 (L - a)) = \frac{\lambda_2}{\lambda_1} \tan(\lambda_2 a) \tag{3.11}$$

where

$$\lambda_1^2 = \frac{\frac{1}{E_{frp}\ t_{frp}} + \frac{b_{frp}}{E_c t_c b_c}}{\frac{\delta_a + \delta_p}{\tau_{fp}}} \tag{3.12}$$

$$\lambda_2^2 = \frac{\frac{1}{E_{frp}\ t_{frp}} + \frac{b_{frp}}{E_c t_c b_c}}{\frac{\delta_{up} - \delta_p - \delta_a}{\tau_{fp}}} \tag{3.13}$$

The ultimate shear strength of strip type anchors that uses elastic brittle interface behavior, named hereafter as “approximate model”, is given in Eq.(3.14).

$$P_u = \sqrt{\tau_{fp} \delta_{up}} \sqrt{E_{frp} t_{frp}}\, b_{frp} \tanh(\frac{\theta\ L}{L_e}) \tag{3.14}$$

where

$$\theta = \sqrt{\frac{\tau_{fp}}{\delta_{up} \sqrt{f_c}}} \tag{3.15}$$

$$L_e = \sqrt{\frac{E_{frp} t_{frp}}{\sqrt{f_c}}} \tag{3.16}$$

L_e is the effective bond length, similar to given in [22] beyond which no strength enhancement is obtained. In Eq.(3.14), τ_{fp} is the shear strength of the plastered layer, b_{frp} is the CFRP width, and δ_{up} is slip displacement as shown in Figure 3.4.

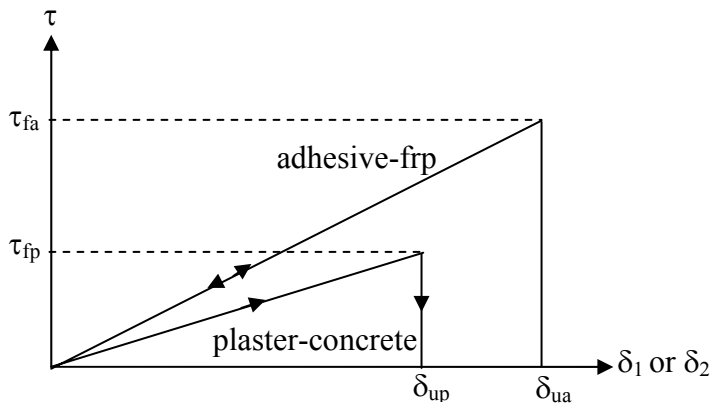

Figure 3.4 τ-δ Relationships Curves of Plaster-Concrete and Adhesive-CFRP Interfaces (Approximate Model)

It should be noted that Eq.(3.10) and Eq.(3.14) can be used to estimate the strength of CFRPs bonded to concrete or HCTs without plaster. For that purpose, τ_{fp} and δ_{up} need to be replaced with the corresponding surface shear strength τ_f and the maximum slip at zero strength δ. These model parameters are estimated according to the calibration of the test results and described below.

3.1.2 Model Parameters

A number of proposals have been previously made [18, 19, 21, 22] to estimate the surface shear strength of CFRPs bonded to concrete. In this study, we adopted Eq.(3.17) proposed by Savioa et al. [24] because it is simple and has proved to yield satisfactory strength estimations.

$$\tau = \omega \ f_c^{\,0.19} \tag{3.17}$$

in their original model for CFRPs bonded to concrete, Savioa et al. [24] proposed the value of ω as 3.5. For HCTs and plastered surfaces, ω is taken as 2 in this study.

For the exact model, the displacement of CFRP anchors bonded to concrete blocks without plaster corresponding to peak strength, δ_a, is taken as 0.051 mm as proposed by Savioa et al. [24]. For the HCTs and plastered surfaces in the exact model, 60% of this value (δ_p=0.03 mm) was used based on engineering judgment. In fact, the model strength estimations are insensitive to this parameter as will be shown with the approximate model.

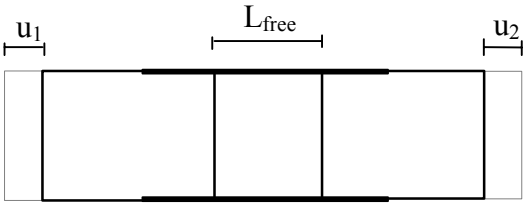

Figure 3.5 Block Deformations

The final parameter is the slip, δ, corresponding to zero interface strength (δ is equal to δ_{up} and δ_{ua} for the specimens with and without plaster, respectively). It can be observed that the interfacial maximum slip, δ, is actually equal to the displacement of the blocks with respect to each other excluding CFRP elongation in the center region (Figure 3.5). In order to extract the ultimate slip, first elastic CFRP elongations corresponding to the unbonded region (center part) are subtracted from the measured maximum relative displacements of the blocks. It should be noted that shortening deformations of the blocks are ignored as they are smaller compared to CFRP elongation.

$$\delta = u_1 + u_2 - \frac{P_u}{A_{frp} E_{frp}} L_{free} \tag{3.18}$$

in which E_{frp} equals to the Young`s modulus obtained from coupon tests on CFRP composite consisting of CFRP sheet and matrix.

In addition to 60 experiments performed in this study, slip values reported by Binici [8] and Nabaka et al. [13] are included to have a total database, containing 103 experiments. The maximum slip is assumed to be a function of the compressive strength of the adherents, ratio of anchor length to effective length and a width ratio. A nonlinear regression analysis is then performed to estimate δ for different cases in form of:

$$\delta = f_c{}^{\alpha}\left(\frac{L}{L_e}\right)^{\beta}\left(\frac{b_{frp}}{b_c}\right)^{\gamma} \tag{3.19}$$

in which b_c is the width of the concrete block or HCT. Exponents α, β, and γ are then found from nonlinear regression analysis and are given in Table 3.1. In Figure 3.6, experimental and calculated slip values using Eq.(3.19) are also presented:

Table 3.1 Coefficients of Displacement Equation

Parameter	Concrete	HCT	Plastered Specimens
α	-0.4	-0.4	-0.4
β	0.80	0.80	0.80
γ	0.40	0.50	0.90

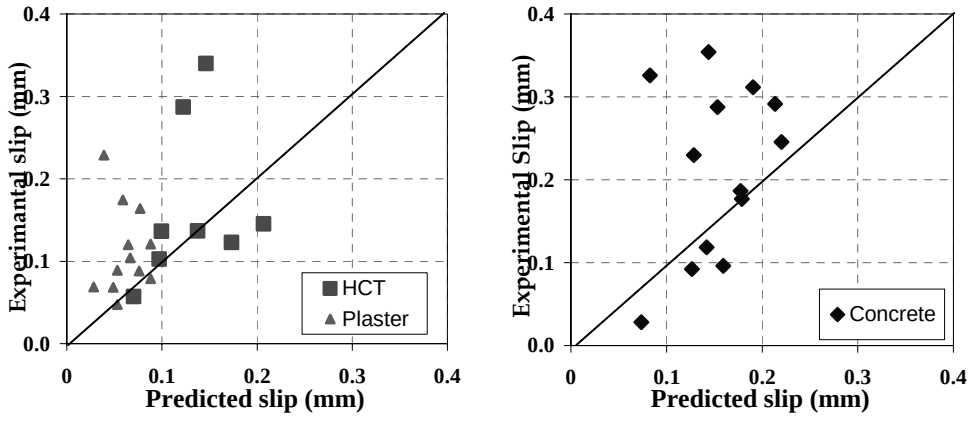

Figure 3.6 Experimental Slip-Predicted Slip Relationships

3.1.3 Model Performances

First, the strength estimation using the "exact" and "approximate" models are compared. The estimated strengths from two models are shown in Figure 3.7 for no-plaster specimens and in Figure 3.8 for plaster finished specimens. It can be observed that both models result in similar strength values for low strength concrete, normal strength concrete, and HCTs with and without plaster.

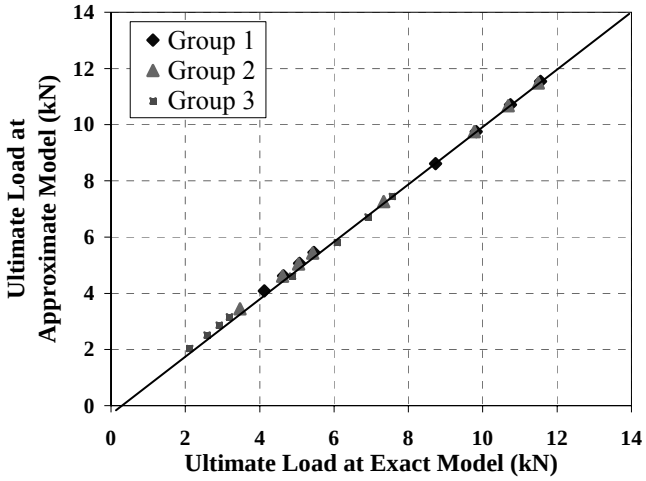

Figure 3.7 Comparison of the Models for Specimens without Plaster

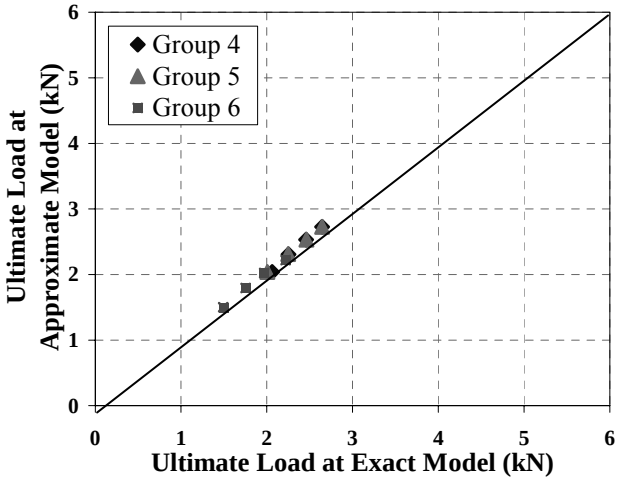

Figure 3.8 Comparison of the Models for Specimens with Plaster

The ultimate shear strength of the specimens calculated by using the approximate model is given in Table 3.2 and the comparison of model and the test results are given in Figure 3.9 and Figure 3.10 for specimens with and without plaster, respectively. It can be observed that the model estimates for the strength of CFRPs bonded to concrete and HCT with and without plaster finish are in good agreement with the experimental results.

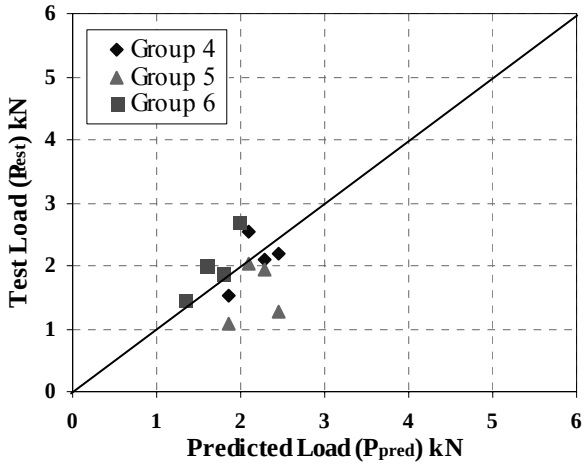

Figure 3.9 Test Load-Predicted Load Relationship of Spe. with Plaster

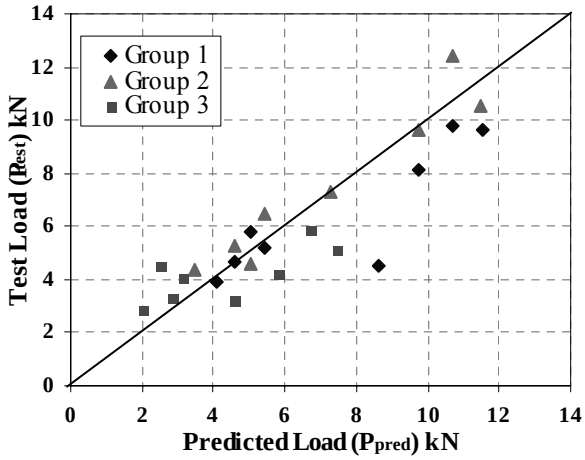

Figure 3.10 Test Load-Predicted Load Relationship of Spe. without Plaster

Table 3.2 Test Loads and Predicted Loads

Specimen	τ	θ	Failure Load P_{test} (kN)	Predicted Load P_{pred} (kN)	P_{test}/P_{pred}
			Group 1		
LCS-1	5.479	3.65	3.88	4.08	0.95
LCS-2	5.479	3.25	4.66	4.62	1.01
LCS-3	5.479	2.97	5.82	5.06	1.15
LCS-4	5.479	2.77	5.17	5.45	0.95
LCS-5	5.479	3.44	4.55	8.61	0.53
LCS-6	5.479	3.07	8.10	9.76	0.83
LCS-7	5.479	2.81	9.81	10.71	0.92
LCS-8	5.479	2.61	9.65	11.54	0.84
Standard Deviation					0.179
Average					0.896
COV					0.200
			Group 2		
NCS-1	6.725	4.04	4.35	3.44	1.26
NCS-2	6.725	3.06	5.30	4.61	1.15
NCS-3	6.725	2.80	4.58	5.04	0.91
NCS-4	6.725	2.61	6.49	5.42	1.20
NCS-5	6.725	3.82	7.27	7.26	1.00
NCS-6	6.725	2.89	9.63	9.75	0.99
NCS-7	6.725	2.65	12.45	10.68	1.17
NCS-8	6.725	2.46	10.55	11.49	0.92
Standard Deviation					0.136
Average					1.074
COV					0.127
			Group 3		
TS-1	2.813	4.04	2.84	2.04	1.39
TS-2	2.813	3.43	4.48	2.52	1.78
TS-3	2.813	3.06	3.35	2.87	1.17
TS-4	2.813	2.80	4.06	3.16	1.28
TS-5	2.813	3.40	3.20	4.61	0.70
TS-6	2.813	2.89	4.21	5.81	0.73
TS-7	2.813	2.57	5.90	6.71	0.88
TS-8	2.813	2.35	5.14	7.44	0.69
Standard Deviation					0.396
Average					1.077
COV					0.368

Table 3.2 (continued)

Specimen	τ	θ	Failure Load P_{test} (kN)	Predicted Load P_{pred} (kN)	P_{test}/P_{pred}
			Group 4		
LCSP-1	2.665	4.86	1.53	1.85	0.83
LCSP-2	2.665	4.33	2.54	2.09	1.22
LCSP-3	2.787	3.91	2.08	2.28	0.91
LCSP-4	2.787	3.64	2.19	2.46	0.89
Standard Deviation					0.174
Average					0.962
COV					0.181
			Group 5		
NCSP-1	2.665	4.38	1.07	1.85	0.58
NCSP-2	2.754	3.87	2.04	2.09	0.98
NCSP-3	2.754	3.54	1.93	2.28	0.84
NCSP-4	2.787	3.28	1.26	2.46	0.51
Standard Deviation					0.217
Average					0.728
COV					0.299
			Group 6		
TSP-1	2.665	5.89	1.46	1.35	1.46
TSP-2	2.665	5.01	1.99	1.60	1.99
TSP-3	2.690	4.45	1.88	1.80	1.88
TSP-4	2.665	4.09	2.69	1.97	2.69
Standard Deviation					0.148
Average					1.184
COV					0.125

3.1.4 Comparison with Other Models

The analytical model proposed in this study was also compared with the test data of other researchers and the results are given in Table 3.3 and Figure 3.11. According to the results, model results generally agree well with the data of other researchers but some of the test results do not provide a good estimate for large values of b_{frp}/b_c. The main reason of this phenomenon is the lack of enough number of experiments with slip measurements for large values of CFRP to concrete width ratio that can be used in the regression analysis.

Further experiments with b_{frp}/b_c close to 1 are needed for a better calibration in this range.

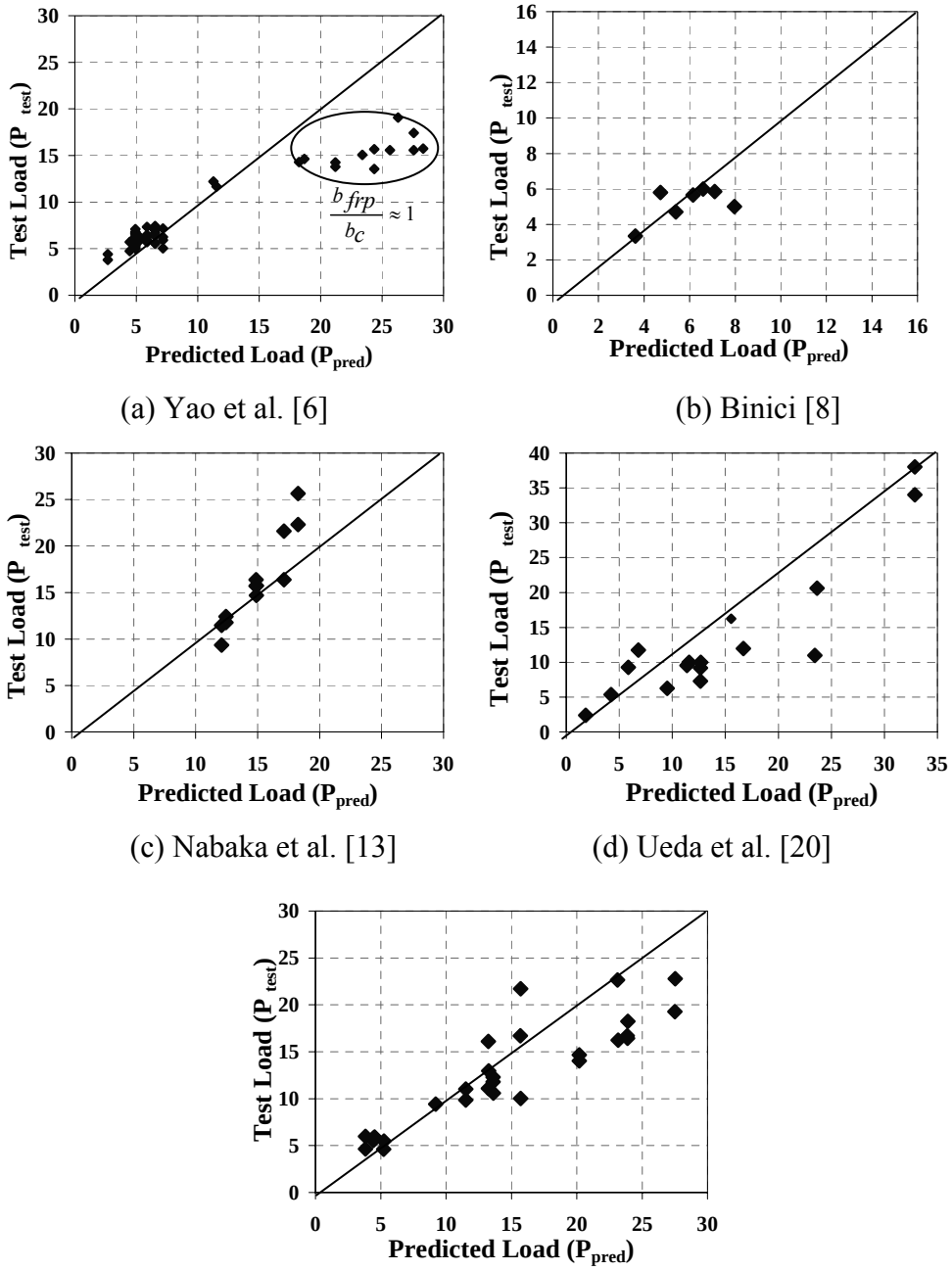

(a) Yao et al. [6]

(b) Binici [8]

(c) Nabaka et al. [13]

(d) Ueda et al. [20]

(e) Ren [25]

Figure 3.11 Comparison of Model with the Data in Literature

Table 3.3 Comparison of the Model with Previous Studies

	Average Predicted-to-Test Bond Strength Ratio	Coefficient of Variation	Standard Deviation
This Study	0.99	0.26	0.26
Yao et al. [6]	1.06	0.23	0.24
Binici [8]	0.90	0.20	0.18
Nabaka et al.[13]	1.06	0.16	0.17
Ueda et al.[20]	0.98	0.36	0.35
Ren [25]	0.98	0.26	0.25

The test results of this experimental study were compared with the analytical model of Maeda et al. [20], Neubauer and Rostásy [21], Chen and Teng [22] and results are given in Table 3.4. It can be observed that the performance of the proposed model in this study provides a better strength estimation with a smaller standard deviation compared to the others.

Table 3.4 Comparison of the Data in This Study with Previous Models

	Average Predicted-to-Test Bond Strength Ratio	Coefficient of Variation	Standard Deviation
This Study	0.99	0.26	0.26
Maeda et al.[20]	0.57	0.45	0.26
Neubauer and Rostásy [21]	0.85	0.30	0.26
Chen and Teng [22]	0.75	0.31	0.23

3.2 EMBEDDED TYPE ANCHORS

A simple model for determining the ultimate shear capacity of CFRP sheets embedded to the concrete specimens was determined based on the test results and the observations in this study.

As mentioned in results of the embedded type anchors section in Chapter 2, for different kinds of concrete strength and different embedded depth obtained, the ultimate shear strength of the specimens without plaster varied around 45%~60% of the full capacity of the CFRP strength. It was observed that the ultimate shear strength of the embedded type HCT specimens without plaster varied around 30%~45% of the full capacity of the CFRP strength. Similarly, the ultimate shear strength of the plaster finished specimens was about 30% of the full capacity of the CFRP laminate.

It is a fact that a simple and working model based on the previous studies on the subject is very important for design purposes to determine the shear capacity. Therefore, a simple and safe model which satisfies the experimental results of specimens with and without plaster derived and given in Eq.(3.20)

$$P_u = \alpha \; t_{frp} b_{frp} f_{frp} \tag{3.20}$$

$$\alpha = \begin{cases} 0.50 & \text{specimens without plaster} \\ 0.35 & \text{plaster finished specimens} \end{cases} \tag{3.21}$$

Where t_{frp}= thickness of the CFRP sheet

b_{frp}= width of the CFRP sheet

f_{frp} = ultimate tensile strength of the of the CFRP sheet

Normalized load-embedment depth relationship of embedded type anchors bonded specimens without and with plaster are given in Figure 3.11 and 3.12, respectively. It can be observed that the use of CFRP embedment increased the efficiency of the material by utilizing it around 50% of its theoretical uniaxial tension capacity.

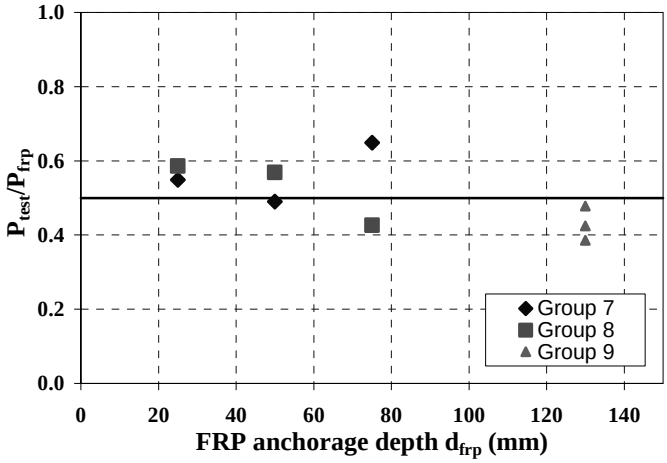

Figure 3.12 Normalized Load-Embedment Depth Relationship of Embedded Type CFRP Anchors Bonded to Specimens without Plaster

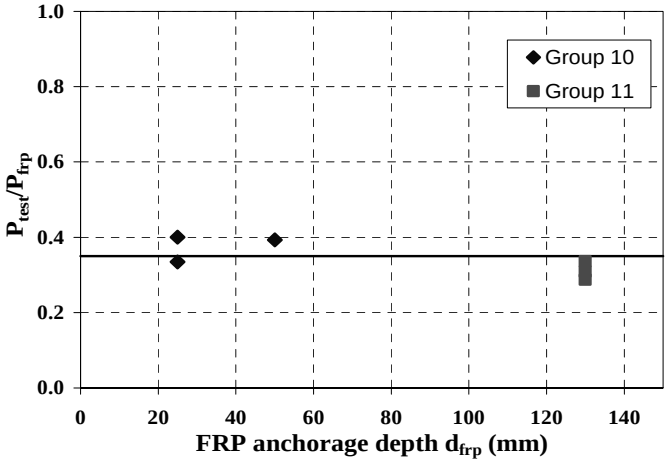

Figure 3.13 Normalized Load-Embedment Depth Relationship of Embedded Type CFRP Anchors Bonded to Specimens with Plaster

CHAPTER 4

CONCLUSIONS

This study presented an experimental study on the bond shear strength of CFRP anchors bonded to concrete and HCT specimens. The effect of plaster on the bonding surface was investigated. The results and the conclusions are presented below:

(1) According to the test results of the strip type anchors bonded to low and normal strength concrete specimens without plaster on bonding surface, main failure mode was concrete failure which generally took place at a few millimeters away from the adhesive-concrete intersection. The bond strength was directly affected from anchorage length, width ratio, and concrete strength. By increasing the bond length up to the effective bond length, the load carrying capacity of the system increased and usually remained constant beyond the effective length. During the experimental program, two types of concrete strength were used to determine the effect of concrete strength. As represented in the study, the effect of concrete strength increase on the ultimate shear strength of bond was limited.

(2) For the strip type anchors bonded to hollow clay tile specimens without plaster on bonding surface, similar observations of effective length, width ratio, and anchorage strength capacities with concrete were obtained. However, lower anchorage strengths were obtained, which was about half of those from concrete specimens, due to weak tile cross-section and discontinuities of the tile surface. Debonding in tile failure mode was dominant.

(3) According to the test results of the strip type anchors bonded to low, normal strength concrete, and hollow clay tile plaster finished specimens, the effect of plaster was found to be significant. Generally, debonding of CFRP from plaster surface was observed. In some of the tests, debonding of the plaster from block surface was also seen due to weak interface between plaster and block interfaces. Anchorage strength capacitates were about half of the specimens without plaster. The effects of plaster thickness and strength were limited because intersection properties between block and plaster cause failure in very small loads which avoid estimating the effects of plaster thickness and strength.

(4) As a result of the embedded type anchors bonded to low, normal strength concrete, and HCT specimen tests with and without plaster on bonding surface, anchorage strength values increased up to two times more compared to the specimens with no special anchorage. Concrete strength effect becomes negligible and similar ultimate loads have been obtained for both low and normal strength concrete. Main rupture mode was the failure of CFRP. The effect of embedment depth was also investigated as a parameter and similar load carrying and displacement capacities were obtained for different embedment lengths. It can be observed that the use of CFRP dowels are practical and can enhance the strength of CFRPs bonded to concrete blocks and HCTs.

(5) According to the test results of the fan type anchors bonded to low strength concrete, an increase in the spread angle up to 30° results in increase of strength. However, for the spread angles larger than 30°, shear strength capacity decreased due to premature failure of CFRPs around spread corners due to stress concentrations.

(6) A simple strength model was developed whose parameters were calibrated based on the experiments presented in this study and those in the literature. The model was also verified by the test results of other researchers. The results showed that the proposed model is capable of estimating the strength of proposed CFRPs bonded to normal and low strength concrete and HCT with or without plaster finish.

REFERENCES

1. Ozcebe G., Ersoy U., Tankut T., Erduran E., Keskin R.S., Mertol H.C., "Strengthening of Brick-Infilled RC Frames with CFRP", TUBITAK SERU-Structural Engineering Research Unit, Ankara, Turkey, Report No: 2003/1

2. Fleming C.F and King G.E.M., "The development of Structural Adhesives for Three Original Uses in South Africa", Int. Symp. on Synthetic Resins in Building Constructions", Rilem, Paris, 1967, pp 75-91

3. Smith, S.T., Teng, J.G., "FRP-Strengthened RC Beams. I: Review of Debonding Strength Models" Engineering Structures, 2002, 24, pp 385-395

4. Chajes, M. J., Finch, W. W., Januzska, T. F., and Thomson, T. A. "Bond and Force Transfer of Composite Material Plates Bonded to Concrete" ACI, Struct. J., 1993, 93(2), pp 208-217

5. Taljsten B. "Defining Anchor Lengths of Steel and CFRP Plates Bonded to Concrete" Int. J. Adhesion and Adhesives, 1997, 17, pp 319-327.

6. Yao, J., Teng, J.G. and Chen, J.F., "Experimental Study on FRP-to-Concrete Bonded Joints", Composites Part B: Engineerring, 36, 2005, pp 99-113

7. Dai J., Sato Y., Ueda T., "Improving the Load Transfer and Effective Bond Length for FRP Composites Bonded to Concrete", Proc. of Japan Concrete Institute, 24, 2002, pp 1423-1428

8. Binici, B, "Punching Shear Strengthening of Reinforced Concrete slabs using Fiber Reinforced Polymers", Dissertation, The University of Texas Austin, USA, 2003

9. De Lorenzis L., Miller B., Nanni A., "Bond of FRP Laminates to Concrete", ACI, Materials J., 2001, 98(3), pp 256-264

10. Ozdemir, G., "Mechanical Properties of CFRP Anchorages" A Master of Sciences Thesis in Civil Engineering, Middle East Technical University, 2005

11. Kobayashi, K., Fujii, S., Yabe, Y., Tsukagoshi, H., Sugiyama, T., "Advanced Wrapping System with CF-Anchor Transfer Mechanism of CF-Anchor", FRPRSC-5 Conference Cambridge, Non-Metallic Reinforcement for Concrete Structures, 2001

12. Dai, J., Uead, T. and Sato Y., “Development of the Nonlinear Bond Stress-Slip Model of Fiber Reinforced Plastics Sheet-Concrete Interfaces with a Simple Method”, ASCE, Journal of Composites for Construction, 2005, Vol.9, No.1, pp 52-62.

13. Nabaka K., Kanakubo T., Furuta T., Yoshizawa H., “Bond Behavior Between Fiber-Reinforced Polymer Laminates and Concrete” ACI, Struct. J.,2001, 98(3), pp 359-367

14. Lu, X.Z., Teng J.G., Ye, L.P., Jiang, J.J., “Bond-Slip models for FRP Sheets/ Plates Bonded to Concrete”, Engineering Structures, 2005, 27, pp 920–937.

15. Malek, A.M., Saadatmanesh, H., Ehsani, M.R., “Prediction of Failure Load of R/C Beams Strengthened With FRP Plates Due to the Stress Concentration at the Plate End.” ACI, Struct. J., 1998, 95(1), pp 142-152.

16. Brosens, K., and Gemert, D. V. “Anchoring Stresses Between Concrete and Carbon Fibre Reinforced Laminates” Proc. 3rd Inter. Symp. Non-Metallic (FRP) Reinforcement for Concrete Structures, 1997

17. Wu, Z., Yuan, H., Niu, H., “Stress Transfer and Fracture Propagation in Different Kinds of Adhesive Joints”, ASCE, Journal of Engineering Mechanics, 2002, Vol.128, No.5, pp 562-573.

18. Yuan H, Teng JG, Seracino R, Wu ZS, Yao J., “Full-range Behavior of FRP-to-Concrete Bonded Joints”, Engineering Structures, 2004 , 26(5), pp 553–564

19. Maeda T, Asano Y, Ueda T, Kakuta Y. “A Study on Bond Mechanism of Carbon Fiber Sheet.”, Non-metallic (FRP) Reinforcement for Concrete Structures, Proceedings of Third International Symposium, Sapporo, Japan, 1997, pp 279–285

20. Ueda, T., Sato, Y., and Asano, Y. “Experimental Study on Bond Strength of Continuous Carbon Fiber Sheet.” , Proc. 4th Int. Symposium on Fiber Reinforced Polymer for Reinforced Concrete Structures, ACI, Detroit, Mich., 1999, pp 407-416

21. Neubauer U and Rostásy F. S., “Bond Failure of Concrete Fiber Reinforced Polymer Plates at Inclined Cracks-Experiments and Fracture Mechanics Model”, 4th Inter. Symp. FRP Reinforcement for RC Structures, 1999

22. Chen, J.F. and Teng, J.G. “Anchorage Strength Models for FRP and Steel Plates Bonded to Concrete.” ASCE, Journal of Structural Engineering, 2001, Vol.127, No.7, pp 784-791.

23. Holzenkämpfer O., “Ingenieurmodelle des verbudes geklebter bewehrung für betonbauteile”, Dissertation TU Braunschweig, Germany, 1994

24. Savioa M., Farracuti B., Mazzottti D., “ Non-Linear Bond-Slip for FRP Concrete Interface”, Proc. of 6th International Symposium on FRP Reinforcement for Concrete Structures., Singapore, World Scientific Publications, 2003,pp 183-192

25. Ren H.T., “ Study on Basic Theories and Long Time Behavior of Concrete Structures Strengthened with Reinforced Polymers”, Dissertaion, Dalian University of Technology, China , 2003

APPENDIX A

ULTIMATE SHEAR STRENGTH OF STRIP TYPE ANCHORS

As mentioned in Chapter 3 the governing differential equation in the solution of the problem is:

$$\frac{d^2\delta}{dx^2} = \tau\left(\frac{1}{E_{frp}t_{frp}} + \frac{b_{frp}}{E_c t_c b_c}\right) \tag{A.1}$$

Ultimate shear capacity of the strip type anchors bonded plaster finished specimens determined using two different model (exact and approximate) based on the equation given in Eq.(A.1)

A.1 EXACT SOLUTION

For the "exact" solution of the specimen with plaster, analytical solution of Yuan et al [18] is further extended to accommodate the presence of a plaster layer. In their original model, the objective was to obtain the full load-deformation response of a CFRP bonded joint. Conversely, the ultimate strength of the bonded joint is the main focus in this study.

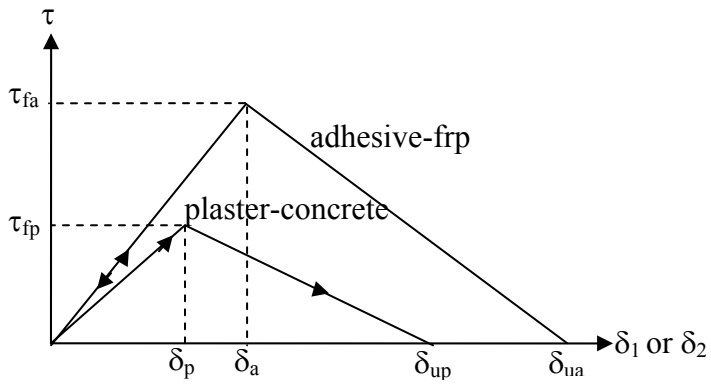

Figure A.1 τ-δ Relationships of Plaster-Concrete and Adhesive-CFRP Interfaces

In addition to the assumptions listed in the Chapter 3, we assume interface stress-slip behavior as presented in Figure A.1 for adhesive-CFRP and plaster-concrete interfaces. Qualitative load-displacement behavior of a CFRP bonded joint is given in Figure A.2. Three basic regions of the curve in the exact model are the elastic part (up to point A), softening branch (between A and B), and debonding stages (beyond point B). In the elastic stage, deformations increase in proportion to the increment of loads and the stress-slip behavior is linear elastic. Once the shear strength of the interface is reached (point A), softening branch is followed in the τ-δ curve beyond a slip value, corresponding to τ_{fa} (or τ_{fp} in the presence of plaster). Upon reaching a slip value corresponding to zero shear strength (δ_{up} or δ_{ua}), strength of the CFRP bonded concrete remains constant. Further increase of deformations result in progressive debonding, which can not be measured unless displacement controlled testing equipment, is used. Therefore, the strength corresponding to a slip deformation at zero interface strength is nothing but the strength of the CFRP bonded to concrete (or HCT).

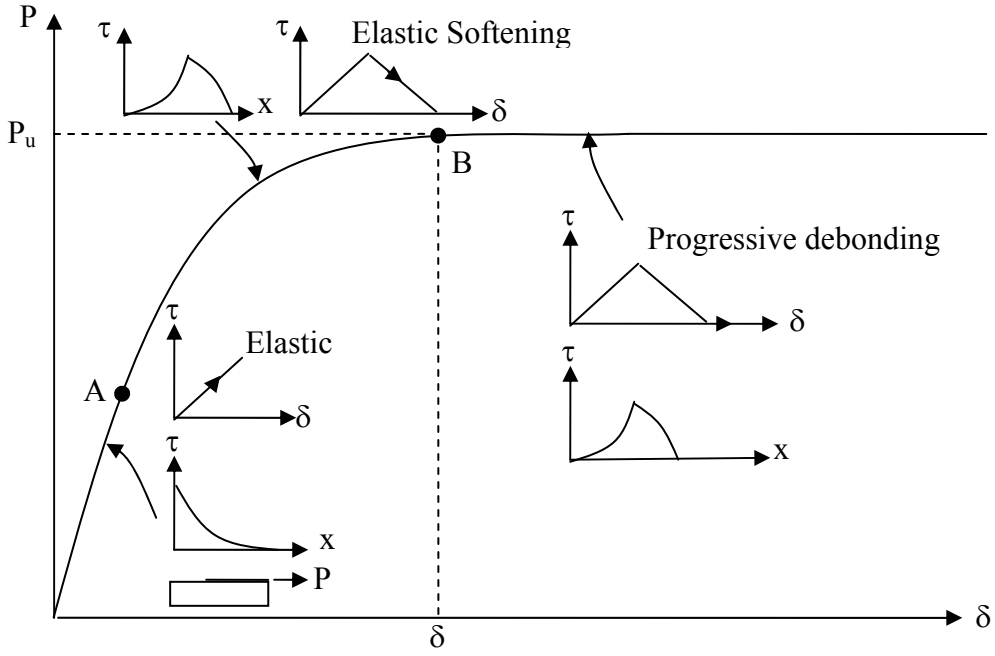

Figure A.2 Load-Displacement Curve of Exact Model

Stress-slip behavior given in Figure A.1 can be given as:

$$\tau = \begin{cases} \dfrac{\tau_{fp}}{\delta_p}\delta_1 & \delta_1 < \delta_p \\ \dfrac{\delta_{up} - \delta_1}{\delta_{up} - \delta_p}\tau_{fp} & \delta_1 > \delta_p \end{cases} \tag{A.2a}$$

$$\tau = \begin{cases} \dfrac{\tau_{fa}}{\delta_a}\delta_2 & \delta_2 < \delta_a \\ \dfrac{\delta_{ua} - \delta_2}{\delta_{ua} - \delta_a}\tau_{fa} & \delta_2 > \delta_a \end{cases} \tag{A.2b}$$

In general, strength of plaster-concrete interface is smaller than the strength of adhesive-CFRP interface. Stress-slip behaviors of the two interfaces are shown schematically in Figure A.1. Accordingly, when the plaster-concrete interface starts softening, adhesive-plaster interface starts unloading to satisfy the condition of similar shear stresses. Therefore, it is reasonable to assume that strength of the plaster governs the interface shear strength in the presence of plaster layer.

Up to the point A of load-displacement curve presented in Figure A.2, both plaster-concrete and adhesive-CFRP interface behaved in elastic range of τ-δ curves of exact model. Slip values of the adhesive and plaster, which is determined from Eqs. (A.2a) and (A.2b), are then given as:

$$\delta_1 = \frac{\delta_p}{\tau_{fp}}\tau \tag{A.3a}$$

$$\delta_2 = \frac{\delta_a}{\tau_{fp}}\tau \tag{A.3b}$$

where

$$\delta = \delta_1 + \delta_2 \tag{A.4}$$

in which δ_1 and δ_2 are slip displacements of plaster and adhesive respectively.

Eq.(A.5) is obtained by substituting Eqs. (A.3a) and (A.3b) in Eq. (A.1)

$$\frac{d^2\tau}{dx^2} - \tau\lambda_1^2 = 0 \tag{A.5}$$

where

$$\lambda_1^2 = \frac{\dfrac{1}{E_{frp}\ t_{frp}} + \dfrac{b_{frp}}{E_c t_c b_c}}{\dfrac{\delta_a + \delta_p}{\tau_{fp}}} \tag{A.6}$$

Solution of the Eq.(A.5) is in the form of:

$$\tau = A\sinh(\lambda_1 x) + B\cosh(\lambda_1 x) \tag{A.7}$$

Using the boundary conditions in Eq (A.8a) and (A.8b), unknown constants A and B can be calculated.

$$\sigma = 0 \quad at \quad x = 0 \tag{A.8a}$$

$$\sigma = \frac{P}{t_{frp} b_{frp}} \quad at \quad x = L - a \tag{A.8b}$$

$$A = 0 \tag{A.9}$$

$$B = \frac{\tau_{fp}}{\cosh(\lambda_1 (L-a))} \tag{A.10}$$

By substituting the unknowns A and B in Eq.(A.7), shear strength and stress of the anchor in the elastic range of τ-δ behavior of exact model, given in Figure A.1 (up to the point A in Figure A.2), is obtained:

$$\tau = \tau_{fp} \frac{\cosh(\lambda_1 x)}{\cosh(\lambda_1 (L-a))} \tag{A.11}$$

$$\sigma = \frac{\tau_{fp}}{\lambda_1\ t_{frp}} \frac{\sinh(\lambda_1 x)}{\cosh(\lambda_1 (L-a))} \tag{A.12}$$

where

$$\frac{d\sigma}{dx} - \frac{\tau}{t_{frp}} = 0 \tag{A.13}$$

In order to describe the region where adhesive-CFRP interface unloads and plaster-concrete interface softens, we use the corresponding softening relationship of the τ-δ relationship. Load at the end of this softening branch is equal to ultimate shear strength of the anchor at point B given in Figure A.2. Slip values of the adhesive and plaster which is determined from Eqs. (A.2a) and (A.2b) are then given as:

$$\delta_1 = \delta_{up} - \frac{\delta_{up} - \delta_p}{\tau_{fp}} \tau \tag{A.14a}$$

$$\delta_2 = \frac{\delta_a}{\tau_{fp}} \tau \tag{A.14b}$$

Substituting Eqs.(A.14a) and (A.14b) in Eq. (A.1), we obtain the governing differential equation in the form of:

$$\frac{d^2\tau}{dx^2} + \tau\lambda_2 = 0 \tag{A.15}$$

where

$$\lambda_2{}^2 = \frac{\dfrac{1}{E_{frp}\ t_{frp}} + \dfrac{b_{frp}}{E_c t_c b_c}}{\dfrac{\delta_{up} - \delta_p - \delta_a}{\tau_{fp}}} \tag{A.16}$$

Solution of the Eq.(A.15) is in the form of:

$$\tau = C\sin(\lambda_2 x) + D\cos(\lambda_2 x) \tag{A.17}$$

Using the boundary and continuity conditions, Eq (A.18a) and (A.18b) constants C and D are calculated as:

$$\sigma = continous \quad at \quad x = (L-a) \tag{A.18a}$$

$$\tau = \tau_{fp} \quad at \quad x = L \tag{A.18b}$$

$$C = \frac{\tau_{fp}}{\sin(\lambda_2 (L-a))} - \frac{\tau_{fp}\lambda_2}{\lambda_1}\tanh(\lambda_1 (L-a))\cos(\lambda_2 (L-a)) - \frac{\tau_{fp}\cos^2(\lambda_2 (L-a))}{\sin(\lambda_2 (L-a))} \tag{A.19}$$

$$D = \frac{\tau_{fp}\lambda_2}{\lambda_1}\tanh(\lambda_1 (L-a))\sin(\lambda_2 (L-a)) + \tau_{fp}\cos(\lambda_2 (L-a)) \tag{A.20}$$

where a is the length along which softening took place. By substituting the unknowns C and D in Eq.(A.17), shear strength of the system at descending branch is found as in Eq.(A.21).

$$\tau = -\tau_{fp}\left[\frac{\lambda_2}{\lambda_1}\tanh(\lambda_1 (L-a))\sin(\lambda_2 (x-L+a)) - \cos(\lambda_2 (x-L+a))\right] \tag{A.21}$$

CFRP stresses are then obtained as in Eq.(A.22) by substituting Eq.(A.21) in Eq.(A.13).

$$\sigma = \frac{\tau_{fp}}{\lambda_2 t_{frp}}\left[\frac{\lambda_2}{\lambda_1}\tanh(\lambda_1 (L-a))\cos(\lambda_2 (x-L+a)) - \sin(\lambda_2 (x-L+a))\right] \tag{A.22}$$

Substituting Eq. (A.23) in Eq. (A.22) and satisfying the condition given in Equation A.23, we obtain applied load P (Eq.(A.24)) as a function of other parameters.

$$\sigma = \frac{P}{t_{frp} b_{frp}} \quad at \quad x = L \tag{A.23}$$

$$P = \frac{\tau_{fp} b_{frp}}{\lambda_2}\left[\frac{\lambda_2}{\lambda_1}\tanh(\lambda_1 (L-a))\cos(\lambda_2 a) - \sin(\lambda_2 a)\right] \quad at \quad x = L \tag{A.24}$$

In order to find the ultimate strength we take the derivative of P with respect to a and equate it to zero to find a corresponding to P_u.

$$\frac{dP}{da} = -\tau_{fp}(1-\tanh^2(\lambda_1(L-a)))\cos(\lambda_2 a) - \frac{\tau_{fp}\lambda_2}{\lambda_1}\tanh^2(\lambda_1(L-a))\sin(\lambda_2 a) + \cos(\lambda_2 a) \quad \text{(A.25)}$$

$$\tanh(\lambda_1(L-a)) = \frac{\lambda_2}{\lambda_1}\tan(\lambda_2 a) \quad \text{(A.26)}$$

The solution of Eq.(A.26) gives a corresponding to P_u and can be found iteratively. Then P_u can be computed as:

$$P_u = \frac{\tau_{fp} b_{frp}}{\lambda_2}\frac{\delta_{up}}{\delta_{up}-\delta_p}\sin(\lambda_2 a) \quad \text{(A.27)}$$

A.2 APPROXIMATE SOLUTION

Determining the "*a*" value by iteration and calculating ultimate load strength in the exact solution is not easy and not very handy for engineers in the design stage of the retrofitting project. By making some simplifications and assumptions on the material model of exact solution, a simple approximate model is proposed to make the bond strength model more practical.

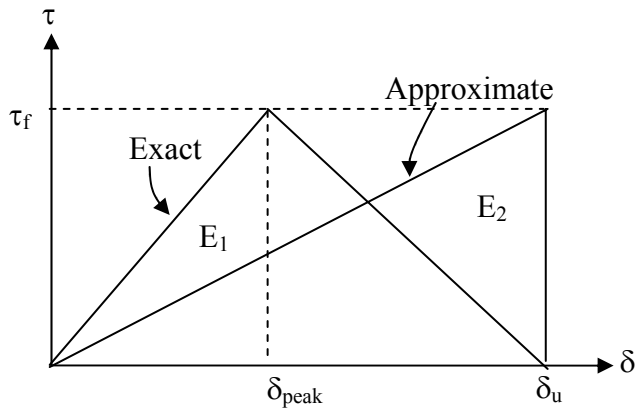

Figure A.3 Fracture Energies of Two Material Models

Both of the material models used in the modeling section are presented in Figure A.3. One of these curves is "exact" behavior of the anchor whereas the other one

is approximate. Area under the stress-strain curves of these two models which can be defined as fracture energy are equal (E_1=E_2). The only difference between the models is the displacements corresponding to ultimate shear capacity of the system. Base on this fact, approximate stress-slip behavior was used to propose a simple model calculating ultimate shear strength of anchor bonded to plastered concrete.

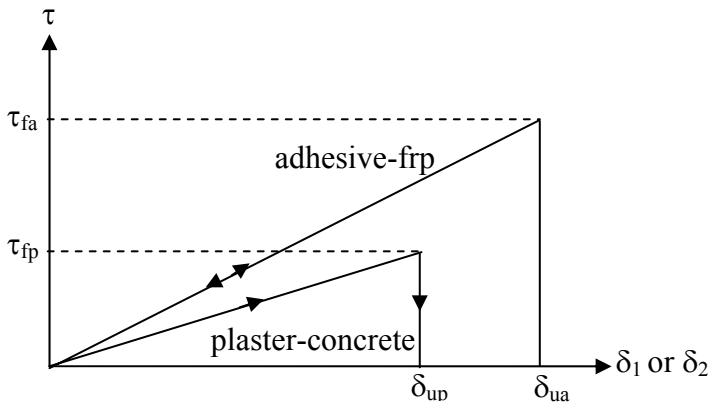

Figure A.4 τ-δ Relationships of Plaster-Concrete and Adhesive-CFRP Interfaces

Stress-slip behavior given in Figure A.4 presented in Eq. (A.28) in form of mathematical expressions.

$$\tau = \begin{cases} \dfrac{\tau_{fp}}{\delta_{up}}\delta_1 & \delta_1 < \delta_{up} \\ 0 & \delta_1 > \delta_{up} \end{cases} \tag{A.28a}$$

$$\tau = \begin{cases} \dfrac{\tau_{fa}}{\delta_{ua}}\delta_2 & \delta_2 < \delta_{ua} \\ 0 & \delta_2 > \delta_{ua} \end{cases} \tag{A.28b}$$

Slip values of the adhesive and plaster which is determined from Eqs. (A.28a) and (A.28b) are equal:

$$\delta_1 = \frac{\delta_{up}}{\tau_{fp}}\tau \tag{A.29a}$$

$$\delta_2 = \frac{\delta_{ua}}{\tau_{fp}}\tau \tag{A.29b}$$

Eq.(A.30) is obtained by substituting Eqs. (A.29a) and (A.29b) in Eq. (A.1)

$$\frac{d^2\tau}{dx^2} - \tau\lambda_3{}^2 = 0 \tag{A.30}$$

Where

$$\lambda_3{}^2 = \frac{\dfrac{1}{E_{frp}\ t_{frp}} + \dfrac{b_{frp}}{E_c t_c b_c}}{\dfrac{\delta_{ua} + \delta_{up}}{\tau_{fp}}} \tag{A.31}$$

Solution of the Eq.(A.30) equal to

$$\tau = E\sinh(\lambda_3 x) + F\cosh(\lambda_3 x) \tag{A.32}$$

With help of boundary conditions in Eq (A.33a) and (A.33b), E and F are calculated.

$$\sigma = 0 \quad at \quad x = 0 \tag{A.33a}$$

$$\sigma = \frac{P}{t_{frp} b_{frp}} \quad at \quad x = L \tag{A.33b}$$

$$E = 0 \tag{A.34}$$

$$F = \frac{P\lambda_3}{b_{frp}} \frac{1}{\sinh(\lambda_3 L)} \tag{A.35}$$

By substituting the unknowns E and F in Eq.(A.32), shear strength of the system at ascending branch is found as

$$\tau = \frac{P\lambda_3}{b_{frp}} \frac{\cosh(\lambda_3 x)}{\sinh(\lambda_3 L)} \tag{A.36}$$

Ultimate load of the anchor is reached at x=L. Hence inserting x=L in Eq.(A.36) gives ultimate load of the system.

$$P_u = \frac{\tau_{fp} b_{frp}}{\lambda_3} \frac{\sinh(\lambda_3 L)}{\cosh(\lambda_3 x)} \tag{A.37}$$

At x=L,

$$P_u = \frac{\tau_{fp} b_{frp}}{\lambda_3} \tanh(\lambda_3 L) \tag{A.38}$$

With the aim of making simplification in λ_3, concrete effect ignored and slips were in terms of total displacement of the anchor which is equal to ultimate plaster slip. Then:

$$\lambda_3 = \sqrt{\frac{\tau_{fp}}{t_{frp} E_{frp} \delta_{up}}} \tag{A.39}$$

$$\lambda_3 = \frac{\theta}{L_e} \tag{A.40}$$

where

$$L_e = \sqrt{\frac{t_{frp} E_{frp}}{\sqrt{f_c}}} \tag{A.41}$$

$$\theta = \sqrt{\frac{\tau_{fp}}{\delta_{up} \sqrt{f_c}}} \tag{A.42}$$

The ultimate shear strength of anchor can be written in form of;

$$P_u = \sqrt{\tau_{fp} \delta_{up}} \sqrt{E_{frp} t_{frp}} b_{frp} \tanh(\frac{\theta\ L}{L_e}) \tag{A.43}$$